Shape Controlled Synthesis of Ag-Au core-shell and Pd Nanoparticles: Understanding their Potential in SERS and Catalysis

Megha

MS15087

A dissertation submitted for the partial fulfilment of

BS-MS dual degree in Science

Indian Institute of Science Education and Research Mohali

May 2020

Certificate of Examination

This is to certify that the dissertation titled **Shape controlled synthesis of Ag-Au core-shell nanoparticles: Understanding their potential in SERS and Catalysis s**ubmitted by **Ms. Megha (Reg. No. MS15087)** for the partial fulfillment of BS-MS dual degree program of the Institute, has been examined by the thesis committee duly appointed by the Institute. The committee finds the work done by the candidate satisfactory and recommends that the report be accepted.

Dr. Ujjal K Gautam **Dr. Arijit Kumar De** **Dr. Debrina Jana**

(Supervisor)

Dated:

Declaration

The work presented in this dissertation has been carried out by me under the guidance of Dr. Debrina Jana at the Indian Institute of Science Education and Research Mohali. This work has not been submitted in part or in full for a degree, a diploma, or a fellowship to any other university or institute. Whenever contributions of others are involved, every effort is made to indicate this clearly, with due acknowledgement of collaborative research and discussions. This thesis is a bonafide record of original work done by me and all sources listed within have been detailed in the bibliography.

Megha Dhiman

(Candidate)

Dated:

In my capacity as the supervisor of the candidate's project work, I certify that the above statements by the candidate are true to the best of my knowledge.

Dr. Debrina Jana

(Supervisor)

Acknowledgment

I would like to express my sincere gratitude to my thesis supervisor Dr. Debrina Jana for her constant support and encouragement throughout the period of my MS thesis. I am feeling blessed for submitting my master thesis under her guidance.

I gratefully acknowledge IISER Mohali for providing me the adequate facilities for doing the research and Department of Science and Technology, India for providing the INSPIRE scholarship throughout the academic program. I gratefully acknowledge INSPIRE faculty research grant of Dr. Debrina Jana for funding this work.

I would like to express thanks to my project committee members Dr. Ujjal K Gautam and Dr. Arijit Kumar De for their valuable discussion and suggestions that improved contents of this dissertation.

I would like to thank IISER Mohali Central and Departmental Research Facility for doing the XRD, TEM and Raman characterization. I am also grateful to Dr. Gurparson Kaur and Mr. Vivek Singh for taking the TEM and FESEM images of all the samples.

I would like to acknowledge Dr. Suman Srivastava from National Institute of Technology, Delhi for carrying out the catalysis part of my project.

I am also thankful to Tinku Ram Meena and Shikha my formal seniors to start the catalysis work which I later continued under their guidance.

I am really grateful to my lab members Ashitha, Dhanvin, Isabella and Abhinil for creating a healthy and cheerful environment in the lab.

Last but the most significant, it gives me immense pleasure to express my gratitude to my beloved parents and family members who have always believed in me and supported with unconditional love throughout my life

List of Figures

List of Tables

Notations and Abbreviations

NPs	Nanoparticles
CTAB	Cetyl Trimethyl Ammonium Bromide
AA	Ascorbic acid
TA	Tannic acid
GA	Gallic acid
NaHS	Sodium hydrosulfide hydrate
EG	Ethylene glycol
PVP	Polyvinylpyrrolidone
PAA	Polyacrylic acid
MB	Methylene blue
$HAuCl_4$	Chloroauric acid
$AgNO_3$	Silver nitrate
$NaBH_4$	Sodium borohydride
PAH	Polycyclic aromatic hydrocarbon
Pd	Palladium
Ag	Silver
Au	Gold

Contents

Abstract

Over decades, plasmonic nanostructures have been used as potential candidate for applications like optoelectronics, catalysis, biosensing, surface enhanced raman spectroscopy (SERS) and many more due to their outstanding optical properties. SERS is a surface dependent technique used to enhance the raman signals up to few orders of magnitude even at single molecular level by taking the advantage of LSPR property of metal nanostructures, making it an excellent platform in chemical and biomedical applications. SERS enhancement mainly depends on anisotropic shape and size of nanostructures. Among plasmonic metals, particularly Ag and Au are used in preparation of SERS substrate owing to their better plasmonic enhancement and biocompatibility. Our main emphasis is to synthesize Ag@Au core-shell nanostructures having spiky shell and smooth shell on hollow Ag@Au and solid Au core. The SERS intensity for each of these morphologies was compared when the target molecule resides in middle of core and shell and on the tips of spiky shell. The intention was to achieve the single molecular sensitivity through these core-shell nanostructures.

Moreover, palladium nanostructures have been used immensely in field of catalysis particularly for carbon-carbon bond formation reactions. Catalytic efficiency have shown the strong reliance on shape and size of nanostructures. So the goal is to synthesize Pd nanostructures of various shapes using capping agent and different reducing agents. The catalytic efficiency of these morphologies was inspected through Suzuki-Miyaura coupling reaction to decipher the relationship between shape and the catalytic activity.

Chapter 1
Introduction

1.1 Plasmonic Metals

Plasmonics is a light-matter interaction concept that involves the interaction of electromagnetic radiation or incoming light with the free electrons on the surface of metal and the dielectric medium (air and glass) that ends up in the generation of electron density wave called plasmons or surface plasmons. These surface plasmons can be defined as collective oscillation of free d electrons of metal in a coherent way between any two materials but the value of permittivity of one material i.e. metal should be positive and other i.e. dielectric should be negative. Surface palsmons can be characterized in to two parts: localized surface plasmon and surface plasmon propagation.

1.1.1 Surface Plasmon Resonance (SPR) and Localized Surface Plasmon Resonance (LSPR)

When a beam of light travels from the air or water or any other dielectric medium reaches the surface of conducting material, underneath specific resonant condition i.e. once frequency of incoming light becomes equal to the natural oscillation frequency of metal, there is a generation of wave at the impinging point of light that travels across the interface referred to as surface plasmon polarization. (Figure 1) Surface plasmon is related to three characteristics distances:

δ_{diel} : Evanescent field in dielectric that represents how far into the dielectric surface plasmon wave will extend.

δ_{metal} : Evanescent field in metal indicates the gap up to that wave will travel into the metal.

δ_{SPP} : Surface plasmon propagation shows how far the wave will move the surface of metal from its excitation purpose.

If the lateral dimension of the interface is less than $\delta_{SPP,}$ the surface plasmon is termed Localised**.** If the oscillation of electron is confined to a particular geometry, it is known as Localized Surface Plasmon Resonace (LSPR). Due to the confinement of surface plasmons to a little space there is no travelling wave and ends up in the localization and enhancement of magnetic attraction field around the surface. Thus solely explicit wavelength will be available for that geometry and it will show maximum absorbance at that wavelength. For noble metals this wavelength lies within the visible region of electromagnetic spectrum, this imparts completely different colors to the metal nanoparticles.

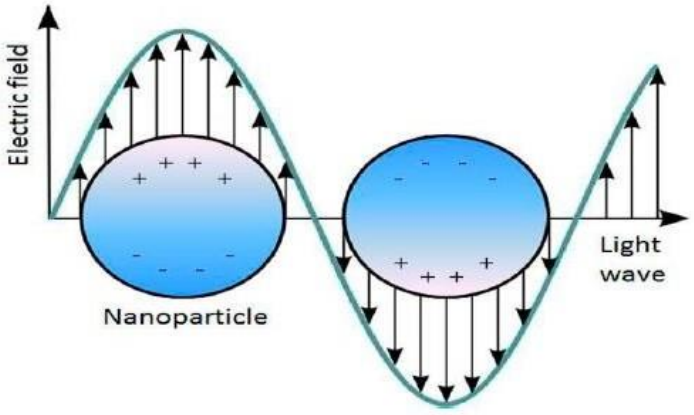

Figure 1. Schematic diagram of LSPR representing the oscillation of free conduction electrons on metal surface due to strong interaction with incident light. (Reproduced from ref.1)

1.1.2 Factors affecting the LSPR of metal nanostructures

LSPR of metal nanostructures rely mostly on size and shape of nanostructures and also on the refractive index of medium and so does the local electric field [2]. Sharp tips and structures having sharp vertices shows higher local field enhancement than spherical due to lightning rod or antenna effect[3]. The electric field density around tips and vertices will not be uniform as in case of spherical nanostructures results in the accumulation of charges and subsequently enhancement of electric field.

When two plasmonic nanostructures come together and form aggregates there is increase in the local field around them[4]. If the separated distance between them is less than their dimension, their plasmons coupled together and results in the amplification of electric field, which is more intense than the individual plasmon intensity[5].

1.2 Surface Enhanced Raman Spectroscopy (SERS)

SERS is a highly sensitive technique that paved the path to enhance raman signal of molecules by taking the advantage of LSPR property associated with nanostructures. This provides the opportunity to overcome the low scattering cross section of raman scatterers and can be used to analyze analytes at ultralow concentrations.

1.2.1 Raman Spectroscopy

Raman spectroscopy is a non-destructive analytical strategy which is used to analyze the chemical structure of compound or quantify a certain substance based on the interaction of light with the covalent bonds present in the substance. It is a light scattering process, where the molecules scatter the incident light coming from high intensity laser source. Maximum of the scattered light has same frequency as that of laser source represents rayleigh scattering that is elastic scattering of photons, whereas some molecules scatter light at different frequency called raman scattering molecules. If these inelastically scattered photons have lower frequency than incident is called stokes shift and higher frequency represents anti-stokes shift.(Figure 2) The raman spectrum thus obtained features a number of peaks and each peak corresponds to a particular molecular vibration thus giving the fingerprint signature of molecules.

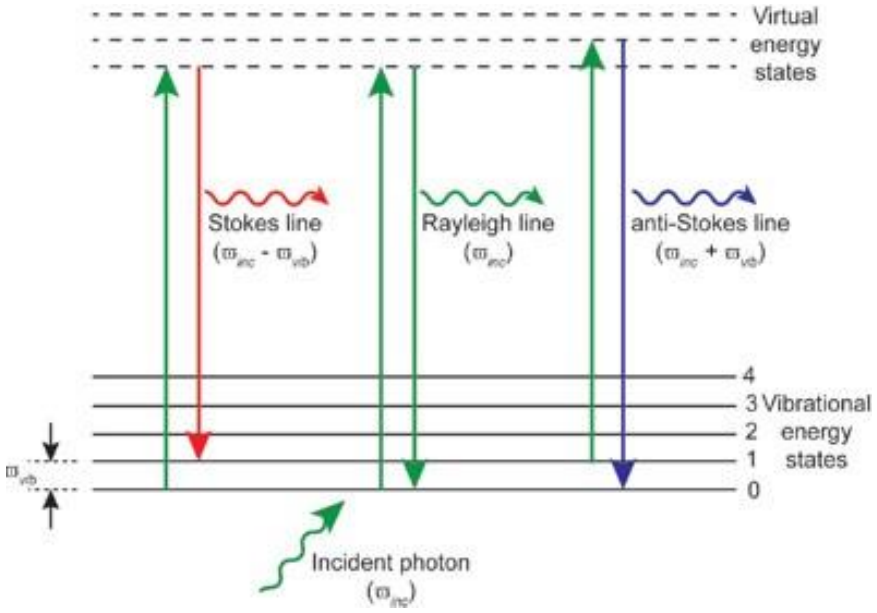

Figure 2. Jablonski diagram representing energy transitions of Rayleigh and Raman scattering (Reproduced from ref 6)

However, only 0.001% photons undergo raman scattering so it is a weak phenomenon. Intrinsically weak raman cross section of molecules limits the wide applicability of raman spectroscopy. To overcome this problem, A. James Mc Quillan in 1974 observed the enhancement in raman signal upto several order of magnitude when pyridine molecules were adsorbed on silver electrode[7]. In 1977 Van Duyne discovered surface sensitive technique called Surface Enhanced Raman Spectroscopy (SERS) and proposed the mechanism also[8].

1.2.2 SERS Enhancement Mechanisms

SERS enhancement is characterized in two mechanisms: Electromagnetic and Chemical Enhancement.

The electromagnetic enhancement occurs when there is excitation of plasmon modes of metallic nanostructures at the equivalent wavelength of the incident light At resonant condition, localized dipoles are created which results in the amplification of local electromagnetic field around the surface of nanostructure.(Figure 3a) When the sample molecules interacts with this enhanced

electric field, there is formation of dipole moments in the analyte molecule that is proportional to the vibrational frequency of molecule[6]. Chemical enhancement originates due to change in polarizability of molecule.(Figure 3b) When sample molecules get adsorbed on to the surface of nanoparticles, transfer of charges takes place between the SERS substrate i.e. metal nanostructure and the target analyte that results in the modification of polarizability of molecule than the individual component[6]. Chemical enhancement factor is peculiar to molecules and shows increment up to the order of 10^1-10^2, whereas EM enhancement can go up to 10^8-10^{12}. SERS enhancement is a combine effect from both EM and chemical enhancement. To calculate the SERS enhancement factor a mathematical equation is used.

$$EF_{SERS} = \frac{I_{SERS}/N_S}{I_{RS}/N_V}$$

I_{SERS} = Intensity of particular raman band of analyte molecule adsorbed on SERS substrate

I_{RS} = Intensity of same band without SERS condition.

N_S, N_V =Average number of molecules in the scattering volume.

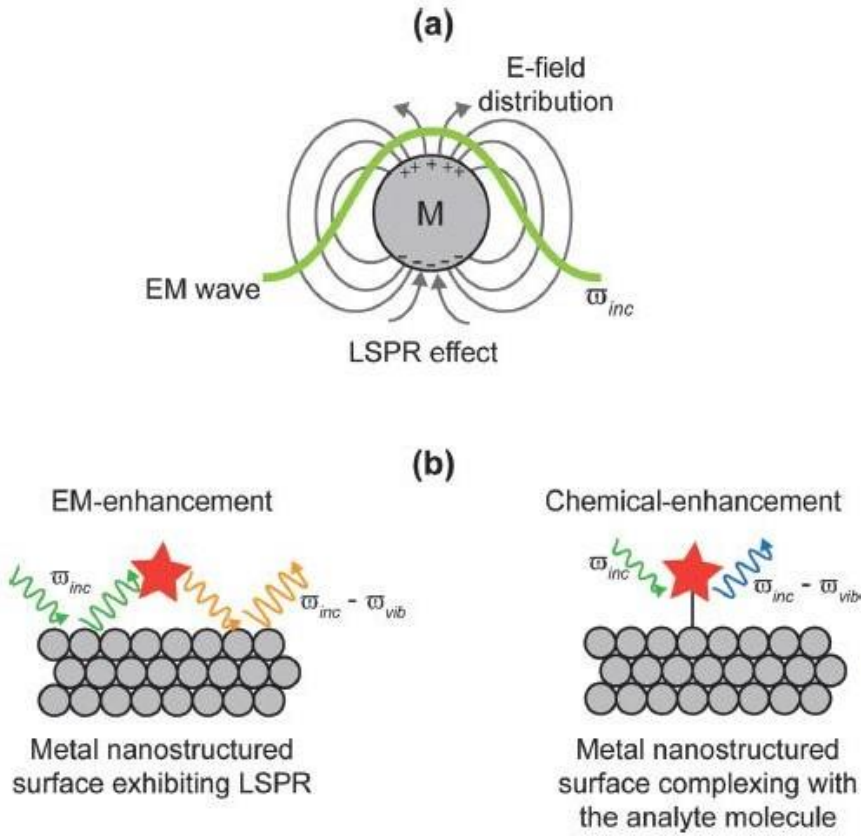

Figure 3. (a) Schematic representation of LSPR effect increasing electromagnetic field around the surface of nanoparticle. (b) Mechanism associated with electromagnetic and chemical enhancement. (Reproduced from ref.6)

1.3 SERS Substrate

SERS enhancement depends on the interaction between the analyte molecules and SERS substrate used. So choosing the suitable substrate plays a pivotal role for increasing the enhancement and hence applications. Mostly the plasmonic metals like Copper (Cu), Silver (Ag) and Gold (Au) are used for the composition because their LSPR peak lies between visible to near infrared region where raman scattering occurs at the maximum level. Cu has oxidation issues in air that impairs its application. Ag and Au proves to be a better candidate having good plasmonic enhancement ability and stability. SERS enhancement mechanisms shows high dependence on shape and size of nanostructures. It has been found that SERS enhancement increases on increasing the size of

nanoparticles[9]. Rui Xiu He et al. have synthesized Ag nanoparticles of size range from 35-65nm and reported that there was generation of strong LSPR and high SERS enhancement as particle size was increased[10]. Researchers have shown that on changing the shape of nanoparticles from spherical to anisotropic shapes with sharp edges enhancement improves because of the presence of non-uniform electric field density around the sharp tips that increases the local electric field and refer to as hotspot[11]. Au metal is known to have good biocompatibility properties so it can be used as a suitable SERS agent for biological samples[12]. Quester et al. have synthesized different shapes of Au nanoparticles like triangles, hexagons, pentagons over a broad size range of 10-200nm and studied their SERS properties[13]. Moreover there are multi-metallic and bi-metallic compositions also that are used as SERS substrate to enhance the SERS intensity mainly, bimetallic includes alloyed nanostructures and core-shell nanoparticles. Alloyed nanostructures have homogenous composition of both the metals at the atomic level. Daohua Sun et al. have reported the synthesis of flower shaped Au-Pd bimetallic nanoparticles showed notable enhancement in SERS intensity and also increased catalytic activity of oxidation of benzyl alcohol[14]. On the other side core-shell nanoparticles having non-homogenous composition where either both metals can be plasmonic or core is made of plasmonic metal covered with silica shell. This can provide chemical stability to the core and also protect from direct contact with probed material which can be useful for biological samples[15]. Thus, tremendous research has been done in field of SERS substrate for better plasmonic enhancement.

1.4 Plasmonic metals in Catalysis

The role of catalyst in any chemical reaction is to increase the rate of reaction by decreasing the activation barrier to form desired product. Plasmonic nanostructures exhibit their LSPR peaks in visible to near infrared region of electromagnetic spectrum that has thrusted their use in increasing the rate and control over chemical transformations. The use of these plasmonic nanostructures in catalysis has increased extraordinary as their properties are better understood. There are number of factors that control the performance of nanocatalyst.

1.4.1 Effect of size: A lot of research has already been done to decipher the effect of particle size on increasing the activity of nanocatalyst. As size of particles decreases, their surface area to volume ratio increases that promotes the increased reactivity as more number of atoms are available on surface to carry out the reaction. This can enhance the catalyst activity and improves the selectivity also. Wilson et al. have reported the synthesis Pd dendrimer encapsulated nanoparticles and studied the effect of particles size on catalytic hydrogenation of allyl alcohol[16]. It was shown that the conversion of allyl alcohol to propanol was fastest when the particle size was smaller. Yang Li et al. have synthesized Pd nanoparticles-graphene hybrids and analyzed their catalytic activity for Suzuki coupling reaction[17]. It was observed Pd-graphene nanoparticles with size 4nm has shown 100% yield with 95% selectivity, which got decreased as size increased.

1.4.2 Effect of shape: Different shapes of nanostructures can help in increasing the catalytic properties due to the specific binding sites and certain crystal facets exposed on the surface of particular shape of noble metals. Silva et al. have reported the synthesis of different shapes of Ag like triangular prism, quasisphere, cubes and wires and showed their order in catalytic activity, triangular prism exhibited maximum activity than cubes and wires having the lowest. This result suggested that catalytic activity increased as (111) facet became more exposed on the surface of triangular prism, reason being (111) facet was least reactive to oxygen as compare to (100) facet[18]. Wang et al. have shown the dependence of shape on catalytic activity of Pd nanocrystals with octahedral, cubes and spherical morphology for the oxidation of carbon monoxide. They have reported that octahedral showed better catalytic activity having (111) facet exposed on the surface than other shapes[19].

1.4.3 Solvent effect on nanocatalyst: Use of different solvents have great consequence on the catalytic efficiency and activation energy of the reaction as it can promote the specific interaction with some crystallographic facets whereas block with the others thus altering the physical and chemical properties. Chowdhury and group have outlined the synthesis of different anisotropic shapes of Pd nanoparticles on using DMF as solvent in the reaction procedure, as being a dipolar aprotic solvent DMF has potential to interact with some specific planes in the nanocrsytals facilitating the formation of various shapes[20].Moreover, particle size can also be tuned on changing the solvent to DMF. Feifei Wang and group have reported the synthesis of Pd

based catalyst using different solvents including ethanol, glycerin and ethylene glycol and showed the importance of solvent in governing the shape, size and dispersity of Pd based catalyst[21].

1.5 Use of Palladium nanostructures in catalysis

Palladium nanoparticles have been immensely used as catalyst in C-C bond forming reactions like Suzuki-Miyaura, Sonogashira, Heck and plenty of other cross coupling reactions because of their cheap cost, gentle reaction condition and can withstand variety of functional groups. These reactions are used industrially at a huge rate for the manufacture of assorted pharmaceutical agents, agrochemicals and plenty of merchandise. Suzuki-Miyaura C-C cross coupling reaction involves combination of derivative of aryl boronic acid and an aryl halide to form biphenyl species over a Pd catalyst and using K_2CO_3 as base under comparatively gentle reaction conditions[22]. Pd nanoparticles are used as economical catalyst due to their high surface to volume ration from their bulk counterpart and facilitates in having low price and ease within the separation of products[23]. Solid supported Pd catalyst can help in the straight forward separation of catalyst and enhance the reusability. Chemical action property of nanocrystals rely on the controlled size and form of the shaped nanostructures. Metallic nanostructures are synthesized using stabilizing and reducing agents which are polymeric in nature. The stabilizing agent will defend the metal nanoparticle catalyst from deactivation and might also give property on interacting with the substrate selectively. The utilization of Pd nanostructures as catalyst have paved the path for surrounding friendly methods using green, perishable reducing and capping agents in the synthesis.

1.6 My Approach

Goal of Project 1

Palladium nanostructures have been used tremendously in the field of nanocatalysis thanks to their optical properties. The catalytic potency depends mainly on shape and size of the nanostructures. So to validate the points that manifest narrow size distribution and well-defined morphology plays crucial role in controlling the catalytic performance and various other properties, the idea was to synthesize the different shapes of Pd nanoparticles using stabilizing agent (CTAB) and different reducing agents (AA, TA and GA) and other is to anticipate the mechanism behind the formation of various shapes. Literature reports have shown Pd nanostructures as an efficient and most promising catalyst to be utilized in C-C bond forming reactions. The catalytic efficiency of the synthesized Pd nanostructures having different shapes were examined through Suzuki-Miyaura C-C cross coupling reaction. The solid supported Pd nanostructures (Pd/γ-alumina) were used as catalyst and the objective was to investigate the shape dependent properties of Pd nanoparticles in catalysis. Which shape would be more effective in completion of the reaction in less time with smart yield and also to check the reusability of the prepared alumina supported Pd catalyst. Moreover, the traditional nanoparticle synthesis strategies involves use of unsafe chemicals and ends up in the formation of toxic byproducts. Hence, there is a necessity of clean and environmental benign procedure for the synthesis of catalyst so that it can be removed easily. By considering the importance of green chemistry, the reducing agents, capping agent and solvent used in the synthesis were all perishable and biodegradable. The synthesis was administered through a green route in an eco-friendly manner.

To accomplish the catalysis work and examine the catalytic efficiency of all different Pd nanostructures synthesized by Suzuki-Miyaura cross coupling reaction, we would acknowledge Dr. Suman Srivastava and group, National Institute of Technology (NIT) Delhi.

Goal of Project 2

Researchers have already done a great extent of research on exploring various type of SERS substrate to increase the SERS enhancement. Among all the discovered substrates, core-shell nanostructures have been used extensively because of their potential to enhance SERS intensity at very low concentration of target molecule. Though Ag shows better plasmonic properties out of other noble metals but is non-biocompatible, while Au is biocompatible and can be used for biological samples. The mechanism behind the enhancement has shown strong reliance on anisotropic shape of nanostructures and literature reports have shown hollow structures to be better than solid for enhancement. So the goal was to synthesize the different morphologies of core-shell nanostructures. We tried to synthesize spiky and smooth shell consisting of Au precursor salt with hollow Ag@Au core and solid Au core. Then the SERS intensity of the individual core-shell structure was compared when the target molecules reside between core and shell based on their structural characteristics. Moreover, difference in SERS intensity was also measured when the dye molecules were adsorbed on the tips of spiky shell with the molecules placed between core and shell. The intention was to explore the potentiality of these core-shell metallic nanostructures for the detection of ultralow concentrations of analyte to achieve single molecule SERS sensitivity. These nanostructures can be used as a promising candidate in applications like pharmaceuticals and biosensing.

Chapter 2

Project 1

Controlling the shape and morphologies of Pd nanostructures by altering the sequence of stabilizing and reducing agents and examine the shape-catalytic efficiency relationship by Suzuki-Miyaura coupling reaction.

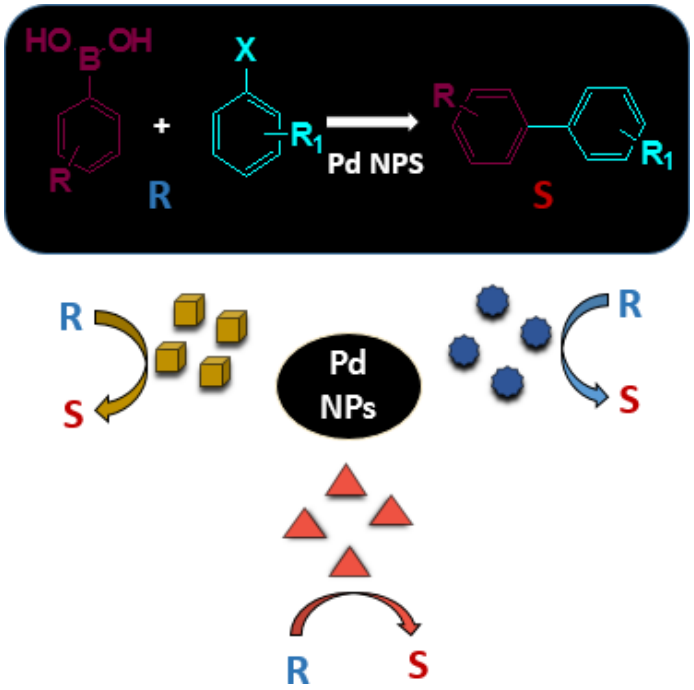

Figure 4. Diagrammatic representation of different morphologies of Pd nanostructures used in catalysis

2.1 Introduction

Among all the plasmonic metals like gold, silver etc. specifically palladium NPs have attracted immense interest due to their wide use in catalysis. The properties of nanoparticle depends both on their shape as well as size. Hence, controlling the shape and size of NPs to improve their performance in application is necessary. Shape dependent synthesis of metal NPs is of pivotal significance to understand the growth mechanism and shape dependent properties. Researchers have made many attempts to synthesize metal nanostructures of different shape by utilizing different stabilizing and reducing agents. Hanfan Liu et al. have synthesized palladium icosahedra by reducing Pd precursor with tetraethylene glycol and PVP as stabilizer[24]. Palladium nanoparticles with nanoplates, nanobelts and nanotrees have readily prepared by using H_2PdCl_2 as precursor and vitamin B_1as reducing agent[25]. Not only using different reducing agents can control the shape of nanostructures but the injection sequence of reducing and capping agent also plays a critical role. Young Lee and group have synthesized Cubic, dendritic and multi armed Pd nanoparticles by just reversing the injection sequence of reductant and stabilizing agent and studied their electrocatalytic activity[26]. Palladium nanoparticles have been considered as most efficient catalyst in vast reactions including the oxidation of carbon monoxide, dehydrogenation of alcohols and water gas shift reaction[27–29]. Opallo et al. have synthesized cubic chain like Pd nanostuctures and showed they have 11.5 times more catalytic activity in fuel cell applications than spherical Pd nanoparticles and commercial Pd/C catalysts[30]. Rong Cao and co-workers have synthesized Palladium nanostructures using cucurbit[n]uril as capping agent and as a support for Suzuki and Heck coupling with high efficiency[31]. Moreover, these solid supported Pd nanoparticles can be easily recovered and can be reused by multiple recycling.

Herein, we report the synthesis of Pd nanostructures by using different reducing and stabilizing agents purely through a green route. The reducing agents (Ascorbic, Gallic and Tannic acid) and capping agent (CTAB) used were environment friendly and biodegradable. The nanostructures of different shape were formed by altering the injection sequence of reductant and capping agent. Meanwhile, the catalytic potential of these Pd nanostructure were analyzed by Suzuki Miyaura reaction to find out the relationship between shape and the catalytic efficiency.

2.2 Experimental Section

2.2.1 Chemicals

Palladium acetate [$Pd(OAc)_2$], Cetyltrimethylammonium bromide (CTAB), Tannic acid, Aluminum-tri-sec-butoxide (ASB), Pluronic F127, Sodium hydrosulfide hydrate (NaSH), were purchased from Sigma Aldrich. Acetone (99.99%) and Ascorbic acid were obtained from SRL. Gallic acid was purchased from Lobachemie. Milli-Q water (resistivity <18.2MΩcm) was used for all purposes. All glass wares used were completely cleaned with aqua regia, washed with distilled water and dried in hot air oven.

2.2.2 Methods

2.2.2.1 Synthesis of Differently Shaped Pd NPs

The synthesis here is characterized in to two parts direct and reverse reaction. The procedure is briefly discussed.

Direct Reaction

0.091g of CTAB was added in 18ml of water in a 100ml round bottom flask. 0.056g of $Pd(OAc)_2$ was separately dissolved in 1.5ml of acetone and added to the prepared CTAB solution. This reaction mixture was placed on an electric heating mantle with refluxing equipment. After approx. 10 minutes, 10 ml of AA (3.7×10^{-2} M) was separately prepared and was added in a reaction at a shot. It was then allowed to reflux and fitted with a condenser. The temperature of the reaction mixture was maintained at 85 ^{o}C. An appearance of dark brownish color was observed after around 30 minutes. The reflux was continued for 45 minutes. In case of tannic and gallic acid, the reaction was done with the same procedure only the concentration of tannic and gallic acid used was 3.7×10^{-5} M.

Reverse Reaction

In this synthesis, 0.056g of $Pd(OAc)_2$ was dissolved in 1.5ml of acetone and added in 100ml round bottom flask. 10ml of AA (3.7×10^{-2} M) was prepared separately and was added in the reaction at a shot. Then the whole mixture was diluted with 3ml of water. This reaction mixture was put on an electric heating mantle. After approx. 10 minutes, 91mg of CTAB was dissolved in 10ml of water and was added in the reaction vessel. It was then allowed to reflux and temperature was maintained at 85 ^{o}C. An appearance of dark brownish color was observed after around 30 minutes. The reflux was continued for 45 minutes. In case of gallic acid, the procedure was same only the concentration used was 3.7×10^{-5}M.

2.2.2.2 Entrapment of Pd NPs inside γ-Alumina for heterogeneous catalysis

6ml of as prepared aqueous solution of Pd NPs was added in 3ml of alumina and kept inside oven for drying overnight. The flakes then formed were used as a catalyst for Suzuki-Miyaura coupling reactions.

2.2.2.3 General procedure for Suzuki-Miyaura coupling

Pd NPs (15mg), K_2CO_3 (3mmole, 414mg), phenylboronic acid (1.1mmole, 134mg)/ 4-methoxyphenyl boronic acid (1.1 mmole, 167mg), aryl halide (1.0mmole) in ethanol (EtOH, 2ml) or in water were placed in the 50ml round bottom flask with magnetic stirring bar under reflux or room temperature respectively. The completion of reaction was observed by thin layer chromatography (TLC). On completion the reaction mixture was concentrated and purified through column with hexane and eluted with hexane and ethyl acetate (9:1). The collected fraction was concentrated and solid was obtained which was dried under vacuum. The purity of product was done through spectral analysis.

2.2.2.4 Procedure for recycling of catalyst

The reaction mixture was centrifuged and the ethanol layer was collected. The washing with ethanol was given two times and then washing was given with water repeatedly for 3 times and was centrifuged. The K_2CO_3 will be dissolved in the water and the nanoparticles will settle at the base. Water layer was decanted and the nanoparticles were collected and dried under reduced pressure. These were reused to check the reusability.

2.3 Characterizations

2.3.1 UV-Visible Spectroscopy

UV- Visible spectra of the aqueous solutions were measured using Cary 5000 UV-Vis NIR (Agilent Technologies) spectrophotometer at the scan rate of 1 nm/s. Quartz cuvette of path length 1 cm at room temperature was used for recording the optical spectra. Baseline correction with corresponding solvent was done every time to eliminate the effect of solvent in the spectrum.

2.3.2 Transmission Electron Spectroscopy (TEM)

Transmission electron microscopy (TEM) studies were carried out using JEOL model JEM-F200 equipped with energy dispersive Xray scattering facility (EDS). The sample for TEM was prepared by drying a drop of aqueous suspension of particles on a piece of carbon coated Cu grid inside hot air oven.

2.3.3 X Ray Diffraction (XRD)

The Pd NPs of different shape and morphology were analysed by X Ray Diffractometer. XRD patterns of samples were measured from Rigaku Ultima IV diffractometer. The sample preparation was done by dropcasting few microlitres of Pd nanoparticle solution on cover slip and kept inside oven for drying or directly small amount of powder sample can be used for XRD. The samples were analysed over an angle range from 30^{o} to 90^{o} at a scan rate of 3^{o}/min. To avoid the background signal from glass, the sample thickness was maintained more than 1μm as the XRD penetration depth was *ca*. 1μm.

2.4 Results and Discussion

Despite the fact that there are numerous studies stating the mechanism of shape conversion of metal nanoparticles, but still there is enough room left for exploring the specific parameters for understanding a particular reaction involving combination of capping, reducing and structural directing agents. In this aspect, keeping in view rapidly growing importance of green chemistry, all the reactions are executed purely through a green route. It is to be noted that all the capping, reducing and structure directing agents are environmental friendly and biodegradable. CTAB and CTAC both can act as green reagent [32,33] but specifically in the reactions described here, CTAB is used as capping agent because it is well known that bromide ion is less corrosive than chloride. The chloride ion in CTAC along with O_2 (present in air) can act as strong etching agent for both nuclei and seeds. Halide ion can change the final shape of nanoparticle by oxidative etching, in which zero valent metal atoms are oxidized back to ions. Presence of more surface defects make multiple twinned seeds highly prone to oxidative environment with their atoms easily being attacked, oxidized and dissolve in the solution, whereas single crystal seeds are resistant for etching. Due to the presence of trace amount of chloride in the reaction all twinned seeds can be removed[34].

Water is employed as green solvent [35]as it is non-toxic, simply accessible, unrequired recycling step, dissolving materials in a wide selection, hindrance of waste and low price. Moreover, the reducing agents used i.e. ascorbic acid[36], tannic[37]and gallic acid[38]are naturally occurring compounds so are environmentally safe and biocompatible.

In all the reactions reported, mild reducing agents are used instead of sturdy reducing agent to convert metal ions into zero valent atom. Stronger reducing agents tend to react in no time and can reduce the metal ions within moments upon addition and leads to the formation of plethora of metal atoms that can directly merge to form larger object via agglomeration, whereas just in case of mild reducing agents, reduction rate is slow and also the concentration of metal atoms steady will increase with time in controlled manner. Once this concentration becomes oversaturated the atoms starts to aggregate into little clusters called nuclei. With a continual supply of atoms these nuclei can grow into nanocrystals. The reduction of Pd^{2+} ions to zero valent Pd^0 atom was confirmed by UV Visible spectroscopy where no characteristic peak showing ligand to metal

charge transfer (LMCT) was observed which implies that all the Pd ions have been converted to Pd^0 oxidation state (Figure 5).

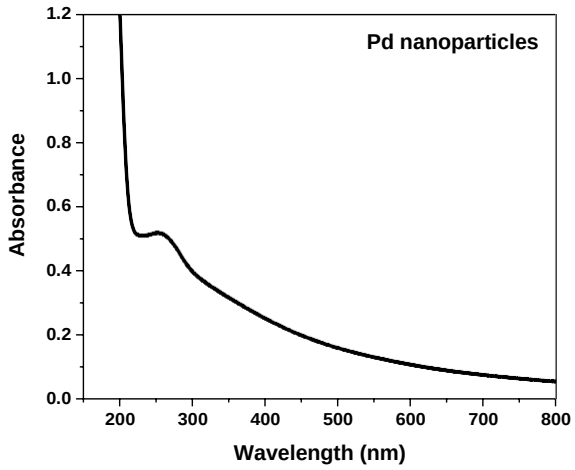

Figure 5.UV-Visible spectra of Pd NPs

In the XRD pattern recorded for three different shapes, there were three peaks observed which can be indexed as reflections arising from (111), (200) and (220) planes of face centered cube of metallic Pd, indicating the crystalline nature of these nanostructures (Figure 6a) and Figure 6b represents the XRD of Pd nanostructures entrapped in the γ-alumina matrix.

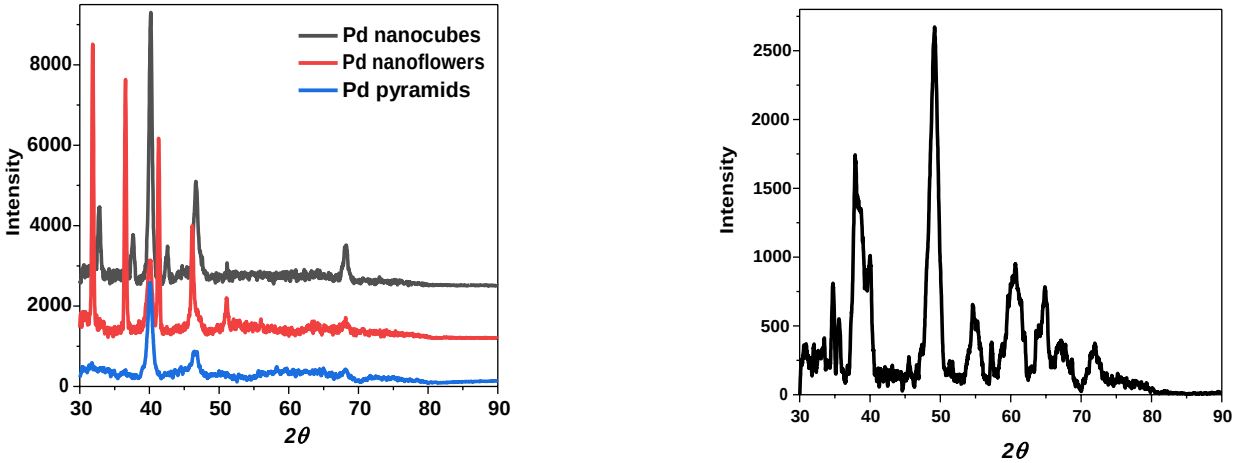

Figure 6. (a,b) XRD peaks of synthesized Pd nanostructures and entrapped inside γ-alumina

2.4.1 Dependence of various factors on morphology of Pd nanostructures

Role of CTAB: CTAB is a cationic surfactant and is used as capping agent for the synthesis of palladium nanoparticles. Since the synthesis is carried out in aqueous solution, the polar head of surfactant will go towards water but metal surface have free electrons so it will also have tendency to bind with the cationic part of surfactant. It has been shown in literature [39]that a bilayer aggregate of CTAB can be formed with the surface of metal, inner layer will bound to metal surface and outer layer will have its polar group towards water and the two layers are interconnected with the help of hydrophobic interactions. Capping agents selectively bind to some facets, making them more stable by reducing their interfacial energy through their unique chemical interaction with the metal surface and control the shape of nanoparticles thermodynamically. The plane with the lower addition is exposed more on the NP surface. CTAB selectively binds to {100} facet of Pd and help in the anisotropic growth of nanoparticles.

The growth of specific shape of nanoparticle consist of two steps nucleation and growth, that involves simple chemistry but is immensely complicated. The crystallinity of seeds plays pivotal role in governing the shape of final product. Seeds may take form of either single twinned, multiple twinned or single crystal, and their population is dependent much more on the size. Use of capping agent can particularly enlarge one set of crystallographic facet over the expense of others to get the final shape. Crystallinity mainly depends on the reduction rate. Injection sequence of stabilizing agent and reducing agent also plays a crucial role in deciding the final morphology of Pd nanoparticles i.e. direct and reverse sequence.

Palladium acetate reacts with CTAB and ascorbic acid in water to give Pd concave nanocubes as evident from TEM images Figure 7 (a,b) when CTAB was added prior to ascorbic acid (Direct sequence) and flower shaped nanoparticles when the injection sequence was reversed i.e. AA was injected first followed by capping agent CTAB as shown in Figure 7 (c,d).

\

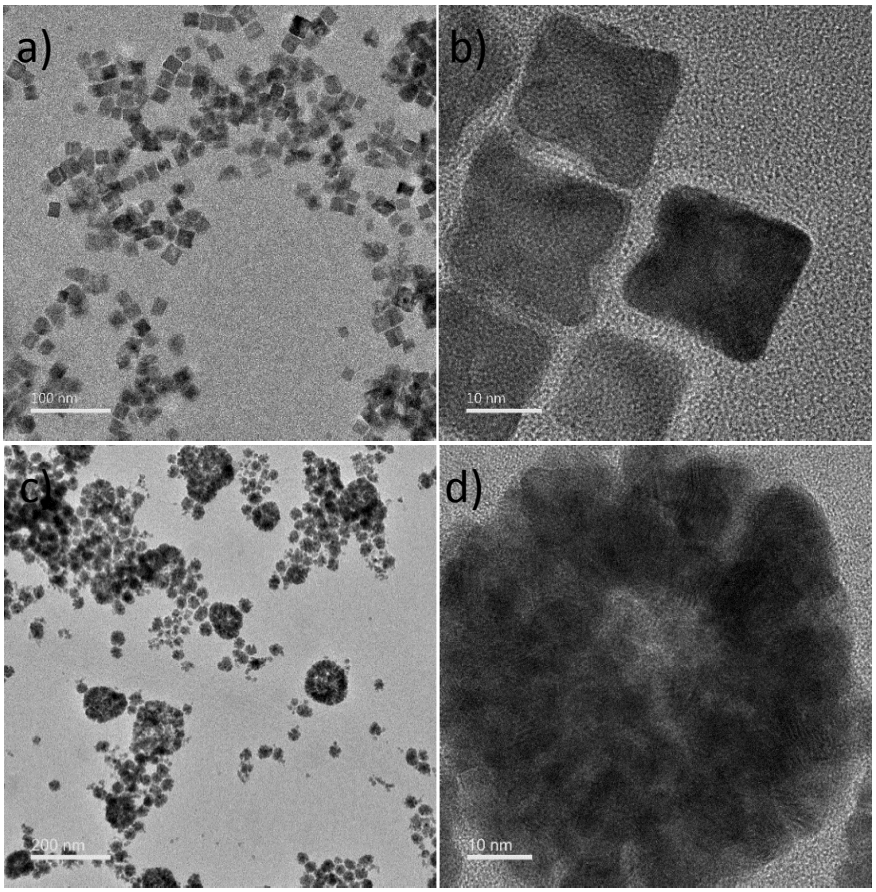

Figure 7. (a,b)TEM images of Pd concave NCs (c,d) TEM images of Flower Shaped Pd NPs.

Ascorbic acid is acting as a mild reducing agent and can reduce Pd^{2+} to Pd^{0} along with its oxidation to 2,3 –diketogulonic acid (2,3 DKG) and series of fragment species simultaneously[40] . AA first reacts with palladium acetate to produce dehydroascorbic acid (DHA) which gets hydrolyzed to 2,3-DKG irreversibly. The formation mechanism of Pd nanoparticles shown in Figure 8 and 9.

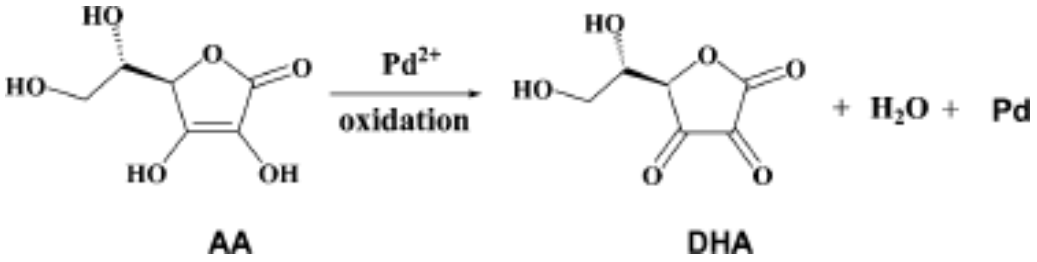

Figure 8. The mechanism for oxidation of AA (Reproduced from ref 40)

Due to the presence of crystalline water in the system, DHA gets hydrolyze to produce 2,3 DKG irreversibly. The conversion of 2,3-DKG to its fragment species can lead to chemical equilibrium moving to the right quickly which accelerates the formation of palladium nanoparticles.

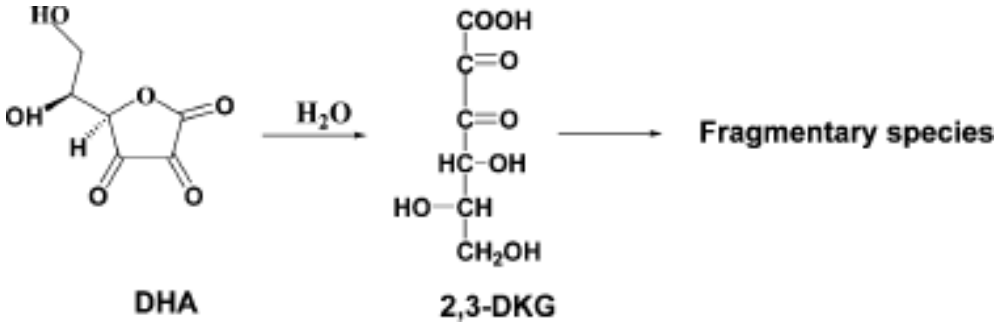

Figure 9. Degradation Scheme of 2,3 DKG (Reproduced from ref. 40)

The formation of different shaped NPs according to the addition sequence of reducing agent and surfactant are often attributed to the regulation of reduction kinetics at the first stage of reaction. When CTAB was added prior to the AA, the resultant form was nanocubes because at the beginning the capping agent will specifically binds to {100} facet of Pd NPs and AA can reduce the Pd ions to generate Pd atoms, which subsequently aggregate to form seeds which will have a selected crystallographic facet exposed on their surface having low surface energy. Most seeds can grow into single crystal and single crystal can evolve into nanocubes which will expose {100} facet [34] and product is under the thermodynamic control.

Whereas, once the sequence of injection was reversed i.e. AA was added prior to CTAB, there was the formation of nanodendrites. AA can cause the quick reduction of Pd precursor and subsequent

increased rate of nucleation and growth of particles. It has been previously stated that large concentration of metal atoms is required for the formation of branched nanoparticles[41,42.] Therefore as a result of fast nucleation and a variety of Pd atoms at the beginning of reaction, the kinetically controlled growth of the seeds resulted in the formation of flower shaped nanostructures[26].It can also be confirmed by TEM images Figure 10, flower shaped nanoparticles have been formed before the addition of capping agent CTAB.

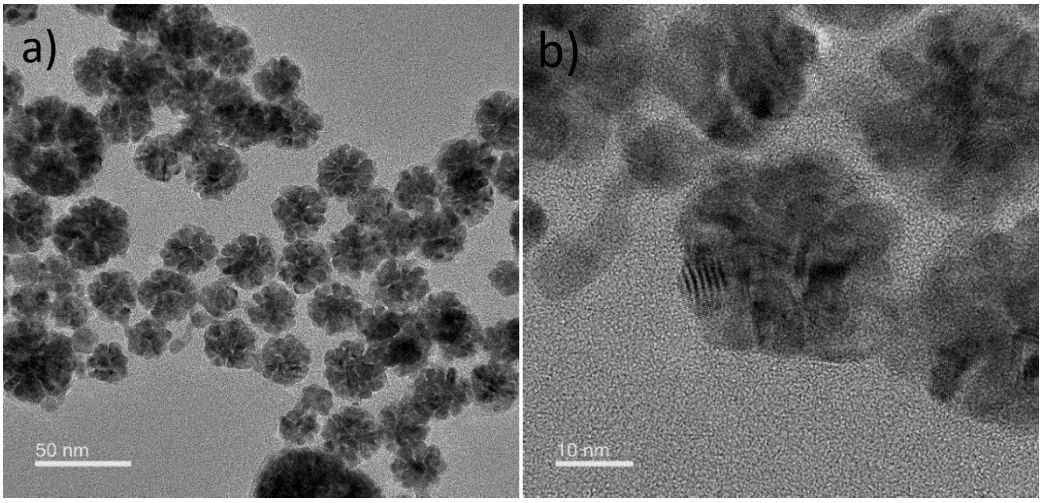

Figure 10. (a,b) Flower shaped NPs before addition of CTAB

Smaller palladium nanopyramids were formed when palladium acetate reacts with CTAB and tannic acid, when the addition sequence was direct as shown in Figure 11 (a,b), whereas reversing the injection sequence results in the formation of larger nanopyramids in the presence of gallic acid and CTAB. Figure 11 (c,d).

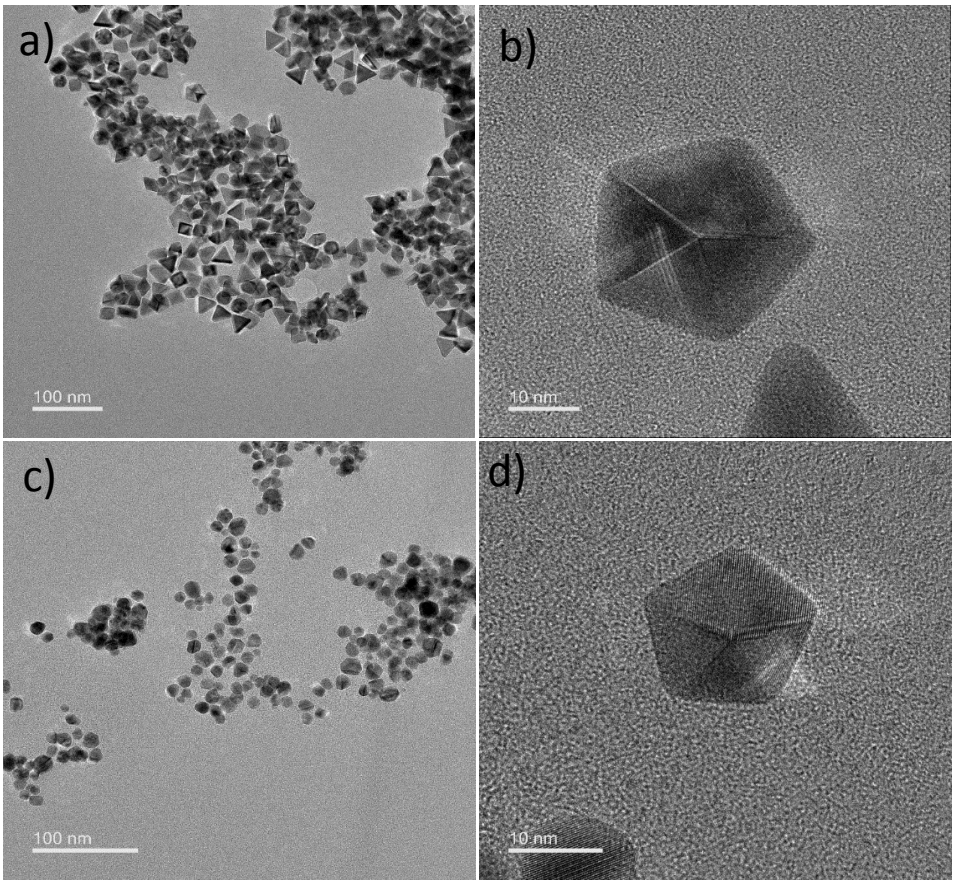

Figure 11. (a,b) TEM images of nanopyramids in presence of tannic acid (c,d) with gallic acid

Tannic and gallic acid are polyphenolic compounds and help in the reduction of Pd^{2+} to Pd^{0} when their phenolic hydroxyl group binds with metal ion and results in five-membered ring formation which subsequently takes part in redox reaction and gets converted to corresponding benzoquinones by donating electrons[43,44]. It can also be noted that Pd^{2+} having high reduction-oxidation potential, shows that Pd(II) can play the role of oxidant when they come in contact with GA Figure 12.

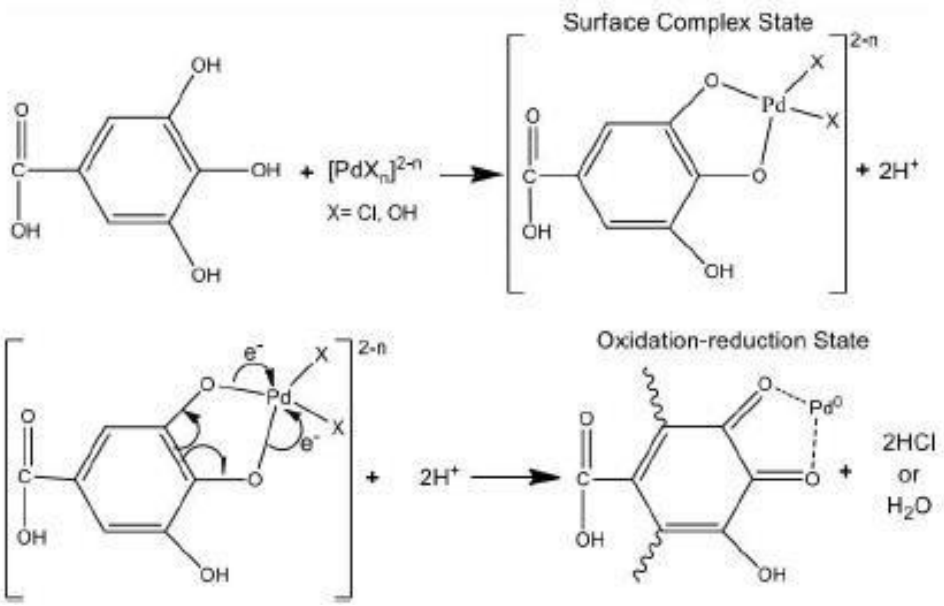

Figure 12. Interaction of gallic acid with Pd(II) ions (X= Cl^-, OAc^-, NO_3^-) (Reproduced from ref. 43)

As tannic and gallic acid are mild reducing agents than ascorbic acid[45] that will result in the slow reduction of precursor salt and consecutively addition of Pd atoms will slow down. Therefore multiple and single twinned seeds can be formed at higher yield in slow reaction. As a result in the growth regime multiple twinned will form icosahedron and decahedron whereas, single twinned seeds evolves into pyramids with particular facet exposed on the surface in the presence of CTAB.

2.4.2 Effect of various factors on catalysis of Suzuki Miyaura Coupling Reaction

Suzuki-Miyaura coupling is characterized by the carbon-carbon cross combination of two aryl subunits, one from derivative of aryl boronic acid and the other from an organohalide to give a biaryl substrate, in the presence of K_2CO_3, ethanol and different shaped Pd NPs as catalyst[46].

Catalyst was impregnated with γ-alumina sol, so that it can separated out easily after the formation of product and can be reused after cycles of reaction. The change in the shape and morphology of catalyst after reusability can be monitored. Figure 13 shows the TEM image of alumina trapped Pd NPs before the reaction.

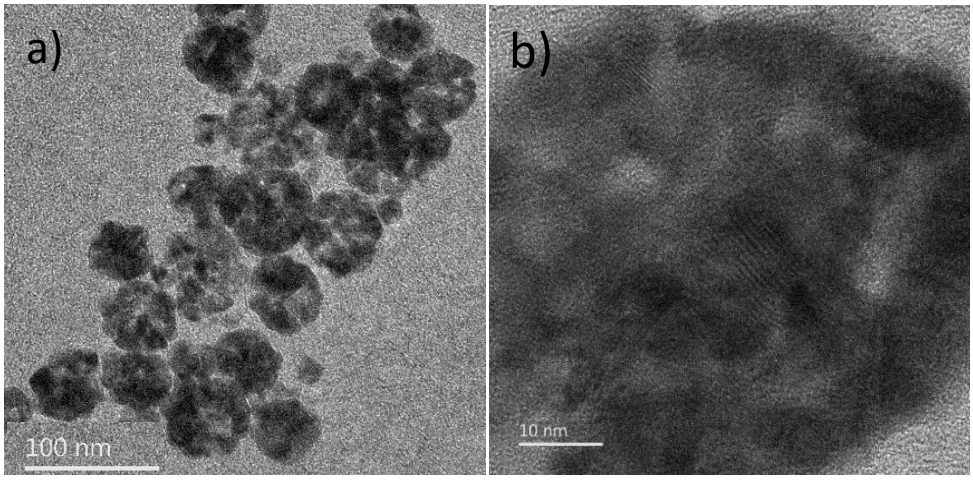

Figure 13. (a,b) Flower shaped Pd NPs entrapped inside alumina sol

2.4.2.1 Effect of Solvent

The experiment was performed to carry out the Suzuki coupling between iodobenzene and phenylboronic acid in the presence of solvent (ethanol or water) and potassium carbonate (K_2CO_3) at 80℃ by using different catalysts (Ascorbic acid (concave shaped, **A**), Ascorbic acid (flower shaped, **B**), Gallic acid (small pyramid, **C**) and Tannic acid (large pyramid, **D**)). Results analysis showed that small pyramids (**C**) found to be the most effective catalyst amongst all as the reaction took place very fast within the first 10 minutes and concave shaped was found to be least effective in ethanol. The same reaction was also performed in the water as solvent and it was found that water act as better solvent in reaction. The reaction was completed faster as compared to the former one. The reaction which was taking 30 or 35 minutes to fully complete in ethanol took the lesser time in the water. Literature showed that water act as green solvent and reduces the use of organic solvent[47]. Arcadi and co-workers used CTAB as the surfactant to increase the solubility of aryl halides showed that the catalyst can be recycled and reused for five cycles with gradual loss of activity[48]. Studies carried out by Lahneche showed that using the water in the effective

concentration leads to increase in the activity but activity started decreasing as the water concentration rises more than 50 mmol as decomposition of catalyst took place[49]. Liu reported the high stability and recyclability of N-hetrocyclic 29arbine-palladium catalyst (HCP-Pd) and found that these are highly active in the water than Poly-Pd due to pyridine group in the HCP-Pd which is more hydrophilic than phenyl group[50]. The reaction was easy to carry out with 95% of yield and there is no change in the activity with the increase or decrease in amount of water. As reported in literature the reaction was all carried out in different solvents as dimethylformamide (DMF), dimethyl ether (DME), acetone, toluene, benzene, tetrahydrofuran (THF) and acetonitrile (CH_3CN) to yield product with >95%. But these solvents were not preferably used as these are time consuming as it took >8 hours to fully complete the reaction[51].

2.4.2.2 Effect of time and temperature

In present study it was seen that different nanoparticles with different shapes and sizes were used to carry out Suzuki coupling reaction in the presence of water or ethanol as a solvent at room temperature or reflux. It was found that reaction easily took place at room temperature when the water is used as solvent but the refluxing (80 ^oC) is needed in case of ethanol as solvent. Water act as good solvent at room temperature and reaction took place at faster rate than in ethanol at refluxing.

Catalyst	**Size (nm)**	**Shape**	**Solvent used**	**Time taken (min)**	**Temperature**	**Yield (%)**
Ascorbic acid (**A**)	25	concave shaped	ethanol	60	80^oC	96
Ascorbic acid (**B**)	60	flower shaped		90		95
Gallic acid **(C)**	15	small pyramid		30		96
Tannic acid (**D**)	35	large pyramid		70		95

Ascorbic acid (**A**)	25	concave shaped	water	60	r.t.	95
Ascorbic acid (**B**)	60	flower shaped		70		95
Gallic acid **(C)**	15	small pyramid		25		97
Tannic acid (**D**)	35	large pyramid		40		96
$Pd(PPh_3)_2$						
$Pd(Oac)_2$						
$Pd_2(dba)_3$ C_6H_6						
$[(\eta^3\text{-}C_3H_5)\text{-}PdCl]_2$						

Table 1. Optimizing the yield of reaction using different solvents and at different temperatures

2.4.2.3 Effect of the shape and size of catalyst

Size and structure of NPs directly affect the activity and rate of reaction. With passage of time the catalyst is recycled and reused over successive runs. It becomes fruitful investigation for controlling the small size of crystals and large surface area as smaller is the size greater will be the activity. In the present work the Suzuki-cross coupling was carried out with **A**, **B**, **C** and **D** nanoparticles having different sizes of 25, 60, 15 and 35 nm. It was found that **C** was most effective and the rate of reaction was fast due to its smallest size as they possess the active surface atom which leads to catalytic performance at higher rate[52]. The nanoparticles having the smaller size (1-3nm) has greater catalytic and recyclability efficiency[53]. Earlier as reported by Molnar that polymer-encapsulated Pd NPs (1–3nm) can efficiently catalyze coupling reactions with minimal leaching with no change in the size and shape of nanoparticle and could be recycled for 7–10 times without loss of efficiency[54].

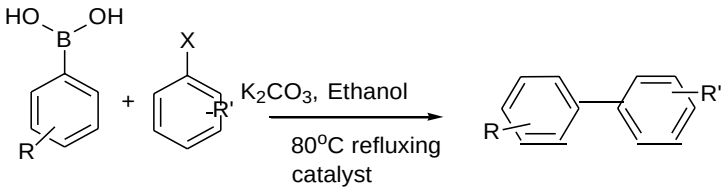

S.no.	R	R’	X	3	Yield (%)
1	H	H	I	3a	97
2	H	OCH_3	I	3b	95
3	H	COOH	3-I	3c	95
4	OCH_3	H	I	3b	96
5	OCH_3	OCH_3	I	3d	95
6	OCH_3	3-CH_3	I	3f	95
7	OCH_3	napthyl	I	3g	94
8	H	H	Br	3a	95
9	H	OCH_3	Br	3b	93
10	H	COOH	3-Br	3c	95
11	OCH_3	H	Br	3b	98
12	OCH_3	OCH_3	Br	3d	95
13	OCH_3	3-CH_3	Br	3e	96
14	OCH_3	napthyl	Br	3f	95
15	H	H	Cl	3a	94
16	H	OCH_3	Cl	3b	95
17	H	COOH	3-Cl	3c	96
18	OCH_3	H	Cl	3b	93
19	OCH_3	OCH_3	Cl	3d	92
20	OCH_3	3-CH_3	Cl	3e	94
21	OCH_3	napthyl	Cl	3f	93

Table 2. Accessing the yield of reaction with different functional groups

TEM studies have shown there was no change in the morphology and shape of catalyst and can be used over successive cycles as catalyst. Figure 14 shows the alumina trapped different shaped Pd nanoparticles after the reaction. Figure 14 (a,b) Flower shaped Al-Pd Nps, (c,d) Concave nanocube shaped NPs (e,f) Larger Pyramid shaped NPs, (g,h) Smaller Pyramid shaped NPs.

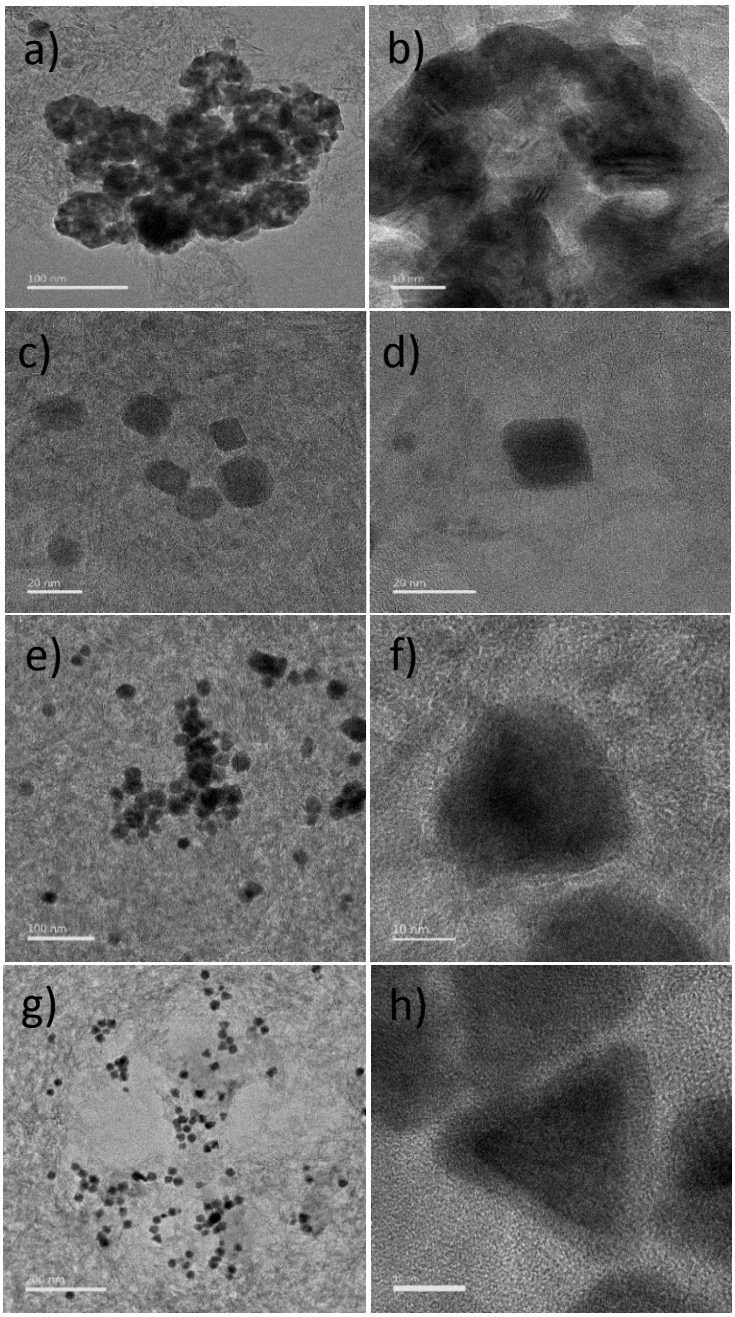

Figure 14. (a,b) Flower shaped Al-Pd NPs , (c,d) Concave NC shape NPs (e,f) Larger Pyramid shaped NPs, (g,h) Smaller Pyramid shaped NPs

EDX (Energy Dispersive X Ray Spectroscopy) studies revealed that the concentration of Pd nanoparticles present in the alumina matrix that is used as catalyst was less whereas maximum concentration was of alumina. Figure 15 shows the EDX of Al-Pd nanoparticles and the quantification of the sample that was on the copper grid.

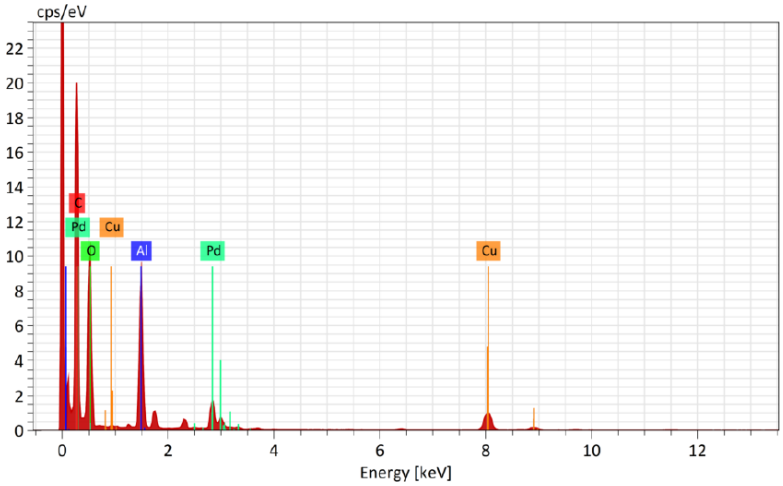

Acquisition.txt

Element	At. No.	Netto	Mass [%]	Mass Norm. [%]	Atom [%]	abs. error [%] (3 sigma)
Palladium	46	4932	39.93	39.93	14.42	4.13
Aluminium	13	141912	60.07	60.07	85.58	5.50
		Sum	**100.00**	**100.00**	**100.00**	

Figure 15. EDX of AL-Pd NPs used as catalyst

Table 3 includes the brief literature survey of the type of Pd nanostructures already been synthesized using various type of supporting material used as catalyst in Suzuki-Miyaura coupling reaction with reported yield, turn over frequency and time taken to complete the reaction.

Catalyst Type	Support Type	Time	Yield	TON/TOF	References
1. Palladium acetate immobilized in thin ionic liquid layers on the mesoporous wall of hierarchical MFI zeolite.	MFI Zeolite	5 hours	Expected : 92% Actual yield: 90%	$3840h^{-1}$	Ref. 55
2.Pd NPs	Fe_3O_4@SiO_2 magnetic nanoparticles	6 hours	95%	$3800h^{-1}$	Ref. 56
3.Pd NPs	Graphene	20 hours	Approx. 100% conversion	230000 TOF	Ref. 57
4.Concave Cube Simple cube shaped Pd	No support	30 hours	80%	$7077h^{-1}$ $1073h^{-1}$	Ref. 58
5.Pd NPs	Al_2O_3 TiO_2 CeO_2	2 hours 2 hours 4 hours	96% 97% 82%	19200 19400 16400	Ref. 59
6.Pd NPs	pEVPBr stabalized	9 hours	95%	-	Ref. 60

7.Pd Nanorods and Branched structure	-	4 hours	90-92%	TOF 14.4 12.5	Ref. 61
8.Poly-Pyrrole Pd Nanocomposite	Polystyrene Microspheres	3 hours	92%	-	Ref. 62
9.Hollow Pd spheres	-	3 hours	99%	-	Ref. 63
10.Pd NPs	Copper oxide	10minutes 150^{o}c	86%	-	Ref. 64
11.Pd NPs	Glycosyl pyridyl-triazole	6 hours	96%	-	Ref. 65
12.Pd NPs	Nitrogen doped Graphene	30minutes	100%	80	Ref. 66
13.Pd NPs	Bipy-PMO	4 hours	98%	-	Ref. 67
14.Pd NPs	Conjugated Polymer Poly(amino	7 hours	96%	TOF EWG 3343 EDG2744	Ref. 68
15.Spherical Pd NPs	Cucurbit[n]uril	20minutes	99%	-	Ref. 69

Table 3. A brief literature survey of different type of Pd nanostructures reported and their use as catalyst in Suzuki-Miyaura coupling reaction.

2.5 Conclusion

We have discussed here that morphologically controlled synthesis of Pd nanostructures depends on crystallinity of seeds and growth of different crystallographic facets. The crystallinity of seeds can be controlled by manipulating the reduction rate and growth of particular facet can be achieved by using different capping agents. The shape controlled formation of Pd nanostructures depends not only on crystallinity of seeds and growth rates but also on controlled reaction sequence. The results here have clearly shown that the reaction sequence is decisive parameter in kinetically controlled synthesis of nanocrystals. The concave NCs, flower shaped NPs, smaller and larger nanopyramids have formed selectively by changing the injection sequence of reductant and surfactant using different reducing agents. To examine the relationship between shape and catalytic performance, thus formed nanostructures have been used as catalyst in C-C bond formation reactions i.e. Suzuki Miyaura Coupling reaction. Result analysis have shown that smaller pyramids found to be the most effective catalyst as the reaction took less time to complete with good yield because of its small size and large surface area. Moreover, TEM images have shown that there was no change in the morphology of catalyst after repeated cycles. This implies that the nanostructures with well controlled shape have better catalytic and reusability efficiency.

Chapter 3

Project 2

Synthesis of different morphologies of plasmonic core-shell nanostructures and probing the SERS of target molecules in the plasmonic confined region.

Hollow Ag@Au core-spiky and smooth shell Solid Au cube core-spiky and smooth shell

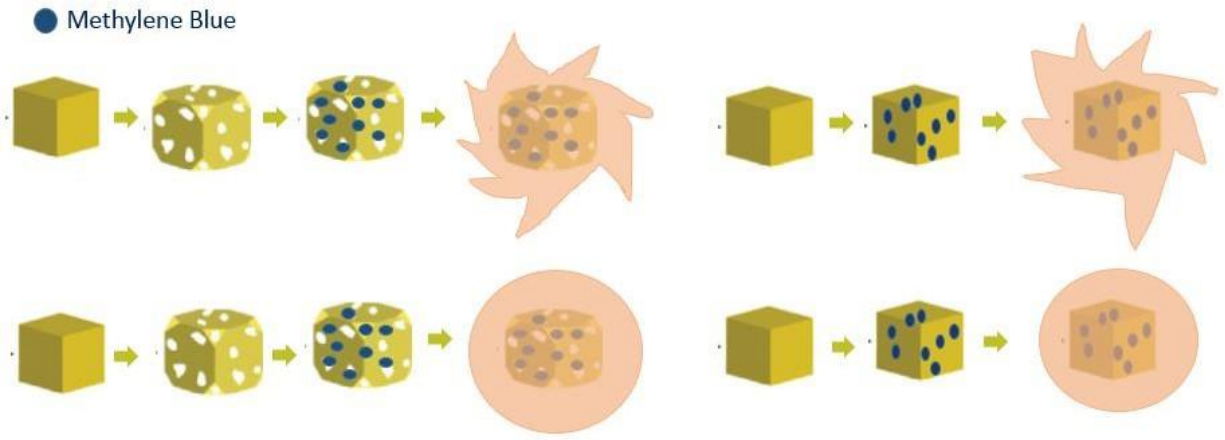

Figure 16. Diagrammatic representation of different morphologies of core-shell nanostructures.

3.1 Introduction

Metal nanostructures have been used thoroughly over decades due to their wide use in applications like catalysis, optoelectronics, pharmaceutical, surface enhanced raman spectroscopy (SERS). Among plasmonic metals, Ag and Au NPs have been extensively used in bioimaging and biosensing[70,71]. Raman spectroscopy gives the fingerprint information of molecules through vibrational excitations but has very weak cross section of molecules that limit its application in detecting very low concentrations. To overcome this problem there was the discovery of Surface enhanced raman spectroscopy (SERS) by Van duyne group in 1977[8]. Since then SERS has become a substantial tool for the detection of molecules adsorbed on the metal nanostructures because of enhanced electromagnetic field called hotspot induced by LSPR (Localized Surface Plasmon Resonance) which involves the collective oscillation of conduction electrons resonated with the particular wavelength of incoming light. LSPR depends on the shape, size of nanoparticles and also on refractive index of medium[2]. Therefore, controlling the morphology and size of nanoparticles has become very crucial. A lot of research has already been done to amplify the raman scattering signals of molecules placed in close proximity to SERS substrate at very low concentrations as well[72]. Several groups have demonstrated that Ag and Au nanostructures with sharp corners and edges can increase the SERS enhancement factor up to several orders of magnitude[73]. Yin Yang et al have reported that hollow nanostructures can increase the SERS activity up to 15 folds than their solid counterparts[74]. Oscar Olea-Mejia and group have synthesized Ag-Au alloy nanoparticles and used them for the detection of methylene blue shows the SERS enhancement up to 360 times higher than when pure methylene blue was analyzed[75]. Zhihui Luo and group have prepared pATP embedded Au/Ag core-shell NPs and used these core-shell NPs as nanotags in SERS immunoassay for the highly sensitive detection of biomarker proteins[76].

No doubt, plasmonic core-shell nanoparticles have potential to exhibit electromagnetic enhancement since the hotspot region between core and shell can be tuned by varying their morphology. Moreover, the location of dye molecules can also be controlled by using spacer molecules through covalent interaction between the core and shell. Lim et al. have used DNA as spacer molecules that can restrict the raman dye molecules between core and shell[77]. They have synthesized core-shell nanoparticles with 1nm gap between core and shell where the dye molecules resides and shows the SERS enhancement with precise dye position and engineered nanogaps.

Researchers have successfully made Au@Au core-shell nanostructures having spiky and smooth shell and have shown the experimental and calculated SERS intensities for probe molecules residing between the core and shell, considerably higher in the structure containing spiky shell, when compared to the smooth shell counterpart[78].

In this work, we have tried to synthesize core-shell nanostructures with different morphology. The spiky and smooth shell with hollow Ag@Au core and second spiky and smooth shell with solid Au core. The SERS signal of the analyte molecules residing between the core and shell for each type of nanostructure was compared. Moreover, the SERS signal from the dye molecules that was restricted between the core and shell with the dye molecules adsorbed on the tips of spiky shell were also compared. It was found that when the dye molecules were placed outside the spiky shell shows greater SERS enhancement as compared to the dye molecules that were in between the core and shell nanoparticles. In addition, the SERS enhancement when the dye molecules were between the core and shell in case of spiky shell with hollow core was higher as compare to the smooth shell- solid core counterpart. Thus the higher SERS signal and large surface area of shell can make these spiky shell-hollow Ag@Au core nanostructures as better SERS nanotags and can be used in therapeutic applications and biosensing.

3.2 Experimental Section

3.2.1 Chemicals

Silver Trifluoroacetate (CF_3COOAg), Tetrachloroauric(III) acid ($HAuCl_4$), Cetyltrimethylammonium bromide (CTAB), Polyvinylpyrrolidone (PVP-55), (MW 55,000), Methylene Blue (MB), Polyacrylic acid (PAA), Polycyclic aromatic hydrocarbon (PAH), Sodium Borohydride ($NaBH_4$), Silver Nitrate (AgNO3), A were purchased from Sigma Aldrich. Acetone (99.99%) and Ascorbic acid were obtained from SRL. Milli-Q water (resistivity <18.2MΩcm) was used for all purposes. All glass wares were thoroughly cleaned with aqua regia, washed with distilled water and dried in hot air oven before use. . All chemicals were used as received without any further purification.

3.2.2 Methods

3.2.2.1 Synthesis of silver cube

In this synthesis, 5mL of EG was added into a flask and heated under magnetic stirring in an oil bath set to 150 °C for 30 min Other reagents used in the reaction were dissolved separately in EG and added with the help of syringe. Sequentially, 0.006 mL (60μL) of NASH solution (3mM) was added first. After 4 min, 0.5mL of HCl (3mM) was added and further followed by 1.25 mL of PVP (20 mg/mL). After 2 min, 0.4mL of CF_3COOAg solution (282mM) was added, the resultant solution was kept for 90 min at 150 °C. Throughout the complete reaction, the flask was capped with glass stoppers aside from the addition of reactants. The synthesis was quenched by placing the flask in an ice-water bath and the products were diluted with acetone and collected by centrifugation.

3.2.2.2 Synthesis of hollow Ag @ Au Cube

0.5mL of prepared Ag cube converted to 2mL by adding 1.5mL water. 0.5mL Ag cube was taken from above diluted solution in 20mL vial. These 0.5 mL Ag NPs dispersed in 3mL of distilled water containing 1mg/mL PVP-55(MW-55000) and heated to 90 °C. After 4-5 min specific

amount of $HAuCl_4$ (10^{-3} M) added and kept for 30 min. The synthesis was quenched by placing the vial in an ice- water bath, then products were collected by centrifugation.

3.2.2.3 Synthesis of Au Cube

Firstly, gold seeds were synthesized by the reduction of gold salts using reducing agent. 0.25ml of $HAuCl_4$ (10mM) was added in 7.5ml of 100mM CTAB solution and solution changed to yellow in color. Color changed instantly to light brown upon addition of 0.8ml of $NaBH_4$. The seed solution was kept undisturbed for 1 hour and then was diluted 1:10 times with water for the synthesis of larger particles. To prepare the growth solution, $HAuCl_4$ (10mM, 0.2mL) and AA (0.95mL) was added into a solution of CTAB (1.6mL) in DI water (8mL). The concentration of CTAB and AA used was 100mM for synthesizing the gold cubes. Then 5µl of seed solution was added and left undisturbed for 15 minutes. The resulting solution was centrifuged and pellet was washed 2-3 times to remove excess of CTAB.

3.2.2.4 Addition of MB dye molecules on the surface of core

The dye molecules were adsorbed on to the surface of core (i.e. hollow Ag @ Au cube and Au cube). 1.5ml of dye solution (10-4 to 10-15 M) was added to the 2ml of core solution and kept for 3h with mild shaking. Then, the solution was centrifuged and precipitate was redispersed in 1ml of distilled water. The solution was then used for the growth of smooth and spiky gold shell on the core.

3.2.2.5 Formation of Smooth Gold Shell on hollow Ag @ Au cubes (Hollow Ag @ Au core- Au Smooth shell structure)

For the formation of a smooth shell on core, 1ml of hollow core solution was added in 0.1mM of PAH dropwise and was kept for stirring around 3 hours. The resulting solution was redispersed in 1ml of distilled water after centrifugation and washing a few times to get rid of excess PAH. Then, 30µL of 10mM $HAuCl_4$ aqueous solution was added to the PAH-coated hollow core particles under vigorous stirring. 50µL of 10mM aqueous AA solution was added to the previous solution after approx. 1 hour and kept stirring for another 12 h. The particles were centrifuged at 14 000 rpm for 10 min and washed a couple of times. Hollow Ag @ Au core−smooth shell nanoparticles were ready to use.

3.2.2.6 Growth of Spiky Shell on hollow Ag @ Au cubes (Hollow Ag @ Au core- Au Spiky shell structure)

For the formation of a spiky shell on the hollow core, firstly the small Ag seeds were grown on hollow core. 1ml of core solution was added to 100µL of 0.01 M $Ag(NH_3)_2$ (prepared by mixing 1 mL of 0.01 M$AgNO_3$ and 20µL of 1M NH_4OH) under constant stirring for 30 minutes. The solution was centrifuged at 14 000 rpm and the precipitate was dispersed in 500µL of doubly distilled water. Then 100µL $NaBH_4$ of 0.01M was added to reduce the adsorbed Ag ions to Ag nanoparticles on the surface of the Au core. The solution was centrifuged at 14 000 rpm for 30 min after keeping 6h for aging. For further growth of spiky shell, a growth solution was prepared consisted of aqueous solutions of CTAB (10mL, 0.1M), $HAuCl_4$ (421µL, 0.01M), $AgNO_3$ (64µL, 0.01M), and AA (67µL, 0.1M). 10µl of the Ag seed solution was added to the growth solution. The color of the solution changed to blue within 15 min and kept for another 2 h with mild stirring. After that the solution was centrifuged and washed 2-3 times to remove excess of CTAB and other reactants. The resultant NPs were redispersed in distilled water.

3.2.2.7 Formation of Smooth and Spiky gold shell on Au cubes (Au core- Au smooth shell and Au core- Au spiky shell structures)

The same procedure as with the hollow core was repeated for the formation of smooth and spiky gold shell on solid Au core.

3.2.2.8 Adding the dye molecules to the outside of Spiky core- shell nanostructures

To adsorb the dye molecules on the outside of spiky core-shell particles, 2ml of NPs solution was added in 1.5 ml of dye solution (10^{-5}M) and was kept for 3 h with mild shaking. The solution was then centrifuged and washed couple of times to remove excess of dye molecules.

3.3 Characterizations

3.3.1 LSPR Measurements

All LSPR measurements were measured using Cary 5000 UV-Vis NIR (Agilent Technologies) spectrophotometer at the scan rate of 1 nm/s. The data was collected by using Carywin software, quartz cuvette of path length 1 cm at room temperature was used for recording the optical spectra. Baseline correction with corresponding solvent was done every time to eliminate the effect of solvent in the spectrum.

3.3.2 Transmission electron microscopy (TEM)

Transmission electron microscopic (TEM) measurements were carried out with Tecnai G^2 30ST (FEI) and Tecnai G^2 20 STWIN (FEI) equipped with energy dispersive X-ray scattering (EDS) facility. For TEM sample preparation, scratched off coatings were dispersed in acetone and drop casted onto the carbon-coated grid.

3.3.3 SERS Measurements

For surface enhanced Raman spectroscopic studies, few microliters of each dispersion was dropcasted on a glass slide covered with aluminium foil to avoid the signal from glass substrate and was kept inside oven for drying. The raman spectra of samples were recorded using Renishaw Raman spectrometer with 20X objective lens. The excitation wavelength used was 633nm equipped with holographic filter with a grating of 1600 lines/mm and 785nm with 1200 lines/mm.

3.4 Results and Discussion

The core-shell structures having smooth and spiky shells were synthesized using solid Au and hollow Au-Ag core, that was consecutively coated within the polymers of alternatively charge using layer by layer charge deposition technique, similar to the other reports shown in literature[79].The probe molecules were coupled using electrostatic interaction to the primary layer of negatively charged polymer. On each polymer deposition, the particles were washed, centrifuged and then resuspended in distilled water. Once few layers of polymer was organized on the surface of solid Au and hollow Ag-Au core, smooth shell was grown using gold precursor and ascorbic acid. To grow spiky shell on the individual cores, there was two step procedure which involves growing small silver seeds on respective cores and then growing spiky shell by addition of CTAB, tetrachloroauric acid, silver nitrate and ascorbic acid. The evidence of formation of Ag NCs, hollow Ag@Au NCs ,smooth and spiky shell on hollow Au-Ag core (smooth shell-hollow NCs, spiky shell-hollow NCs) was confirmed by UV-visible spectroscopy, shown in Figure17 and UV-Visible spectra of Au NCs, smooth and spiky shell on solid Au cube (smooth shell-solid Au NCs, spiky shell-solid Au NCs) shown in Figure18. The observed LSPR peak for smooth shell on the respective cores was red shifted from the peak corresponding to the cores and peak for spiky shells was further red shifted from smooth shell reason being the hybridization of surface plasmon modes occurring between the core and the shell. The LSPR peak for the spiky shell was most red shifted because of the greater field enhancement between core and shell than the counterparts.

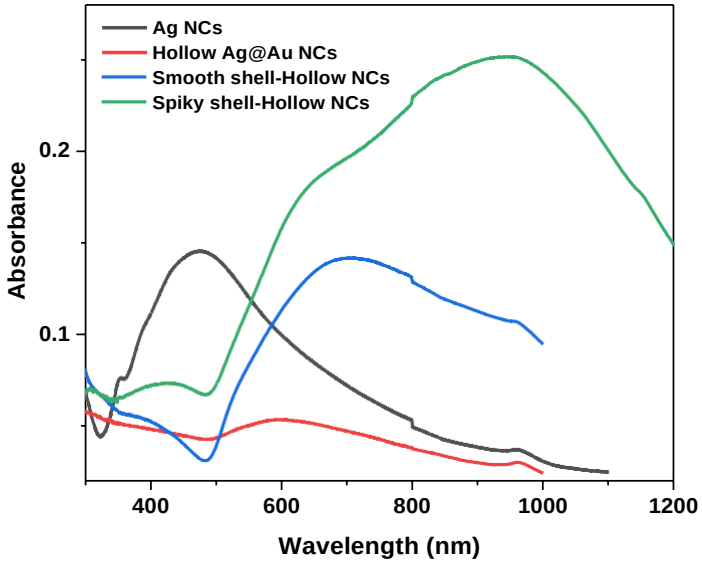

Figure 17. UV- Visible spectra of Ag NCs, hollow Ag-Au NCs, smooth and spiky shell nanostructures

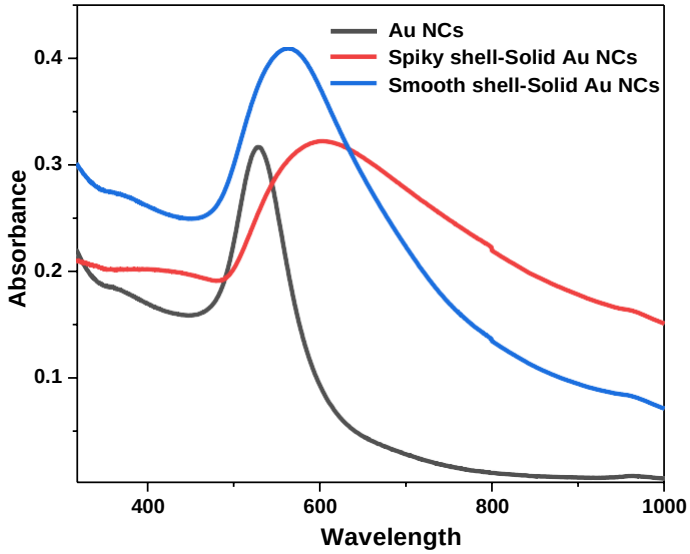

Figure 18. UV-Visible spectra of Au NCs, smooth and spiky shell nanostructures

The morphologies of these core-shell nanostructures was confirmed by using electron microscopy technique. Figure19 shows the TEM images of Ag core and hollow Au-Ag NCs.

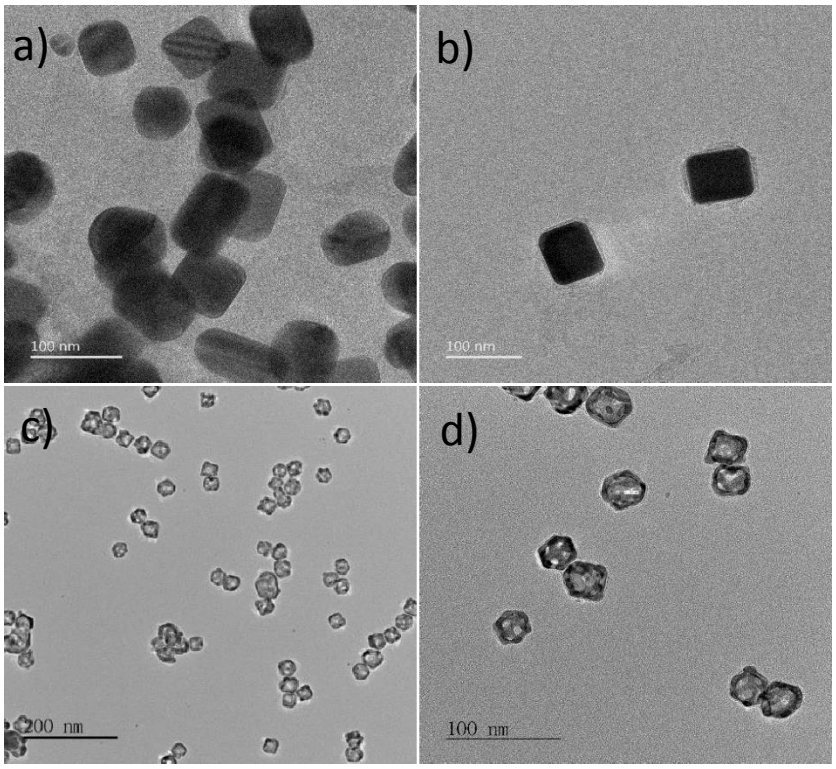

Figure 19. (a,b) TEM images of Ag NCs (c,d) TEM images of hollow Ag@Au NCs

The preparation of these hollow Ag-Au nanostructures was done by adding $HAuCl_4$ through galvanic replacement reaction. In this methodical galvanic replacement procedure (Reduction potential: Ag^+/Ag (0.8V *vs* SHE) & $AuCl^{4-}/Au$ (0.99V *vs* SHE)) the process through which Au-Ag hollow structures are formed is very similar to Kirkendall void formation[80]. The galvanic replacement reaction between Ag NCs and $HAuCl_4$ resulted in the dissolution of Ag atoms firstly from the corners of Ag NCs and then from the interior by oxidation of Ag^0 to Ag^+ ions. One atom of Au deposits at the expense of three Ag atoms. As a result, Ag NCs were transformed into Ag–Au hollow NCs with few Ag remaining in the interiors.

$$3Ag(s) + AuCl^{4-}(aq) \rightarrow Au(s) + 3Ag^{+} + 4Cl^{-}(aq)$$

After adding the dye molecules and polymer deposition, spiky shell of Au was grown on hollow Ag-Au core shown in Figure 20.

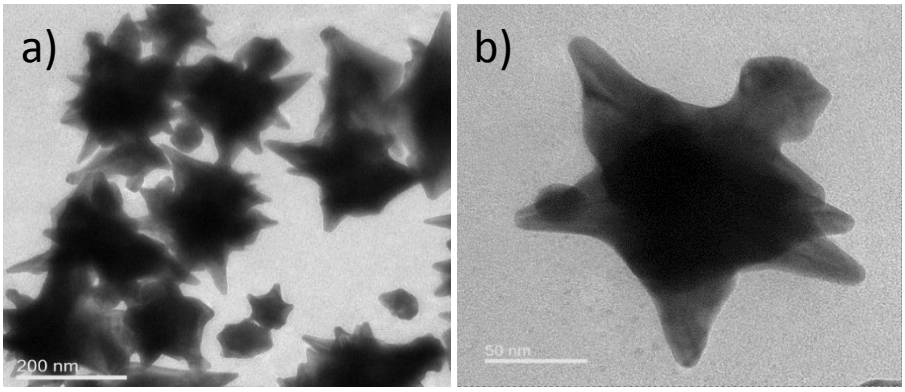

Figure 20. (a,b) TEM images of Spiky shell on hollow Ag@Au core

Figure 21 shows the TEM images of hollow Ag-Au cubes having smooth shell of gold which appears bigger than original core used. Figure 21 (c) shows the energy dispersive X-ray spectroscopy (EDS) elemental mapping image of smooth core-shell structures which indicate the presence of both the metals Ag and Au but the percentage of Au was maximum and Ag was in minute quantity.

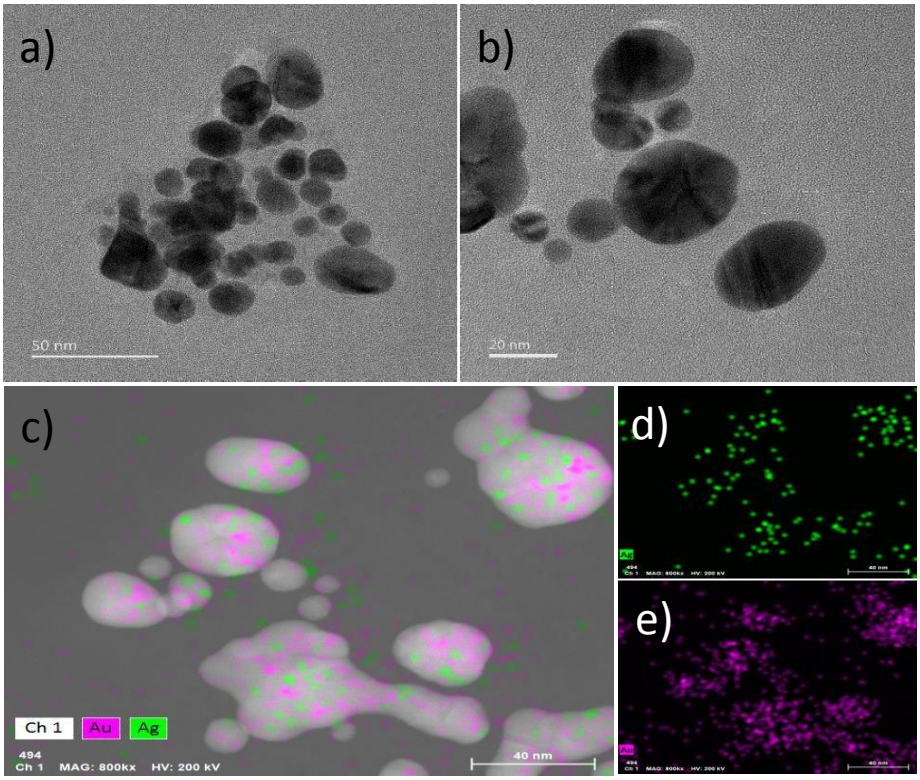

Figure 21. (a,b) TEM images of Smooth shell on hollow Ag@Au core
(c,d,e) Color mapping of Smooth shell nanostructures

The morphology of Au core- shell nanostructures was analysed using SEM images. Figure 22 shows the SEM images of Au cube used as core to grow smooth and spiky shell.

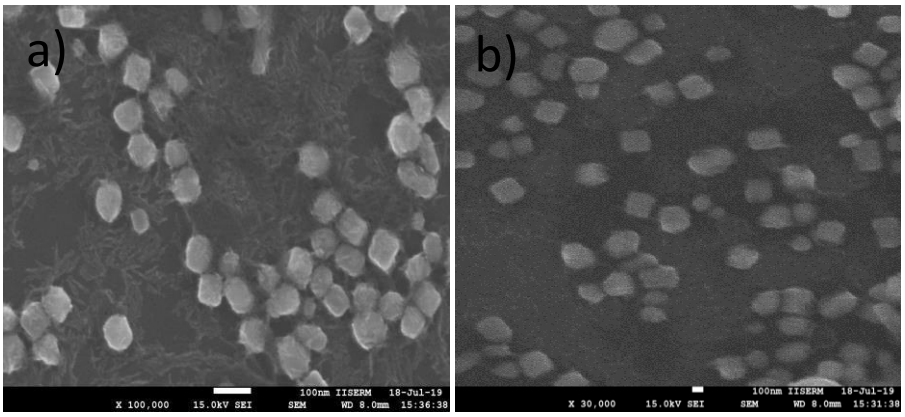

Figure 22. (a,b) SEM images of Au NCs

The Au core synthesized was then used to add dye molecules through polymer deposition. Then smooth and spiky shell of gold precursor was grown on that Au core. The formation of smooth shell on the core was confirmed by SEM as shown in Figure 23.

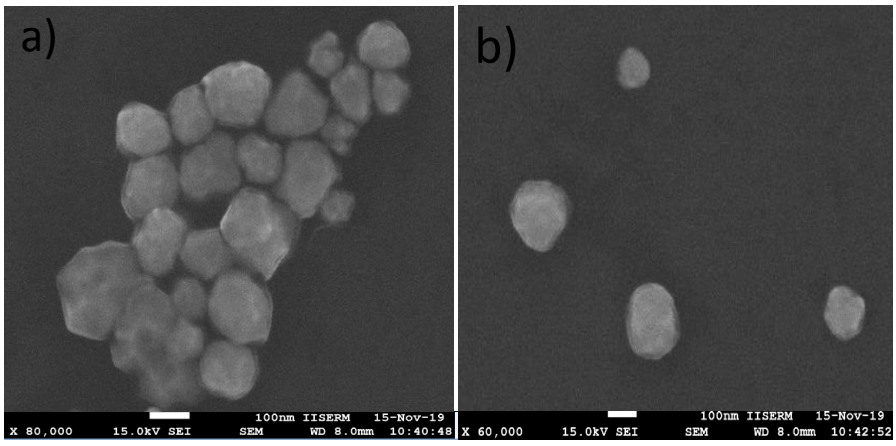

Figure 23. (a,b) SEM images of Smooth shell-Au solid core

3.4.1 SERS Characterization of these core-shell nanostructures

To evaluate the SERS studies of these core-shell nanostructures having smooth and spiky shell on Au and hollow Au-Ag core, MB was used as analyte molecule. MB is an organic dye commonly used in staining and as drug delivery agent. As Ag-Au nanostructures have better plasmonic enhancement and are biocompatible, this makes their SERS study an important aspect. SERS spectra was measured using different type of nanostructures synthesized, spiky and smooth shell-hollow Ag@Au core, spiky and smooth shell–Au core with MB as a probe molecule under 633nm and 785nm excitation wavelength. Figure 24 shows the raman spectra of MB without any substrate i.e. without SERS condition.

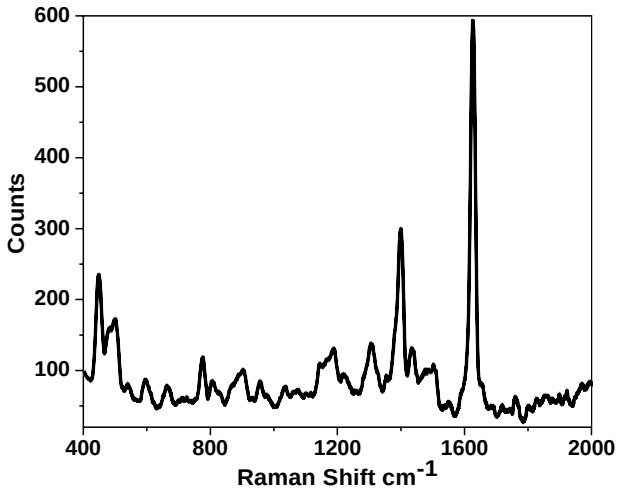

Figure 24. Raman Spectra of MB without SERS condition

SERS spectra of MB molecules between core and shell for both spiky and smooth shell using both the cores were measured to compare their raman enhancement factor. Figure 25 shows the SERS spectra of spiky shell-hollow Ag@Au core at excitation 633nm and 785nm. The concentration of MB was varied from 10^{-3}-10^{-15}M. As the concentration of MB was decreased laser power was increased to get a good raman spectra.

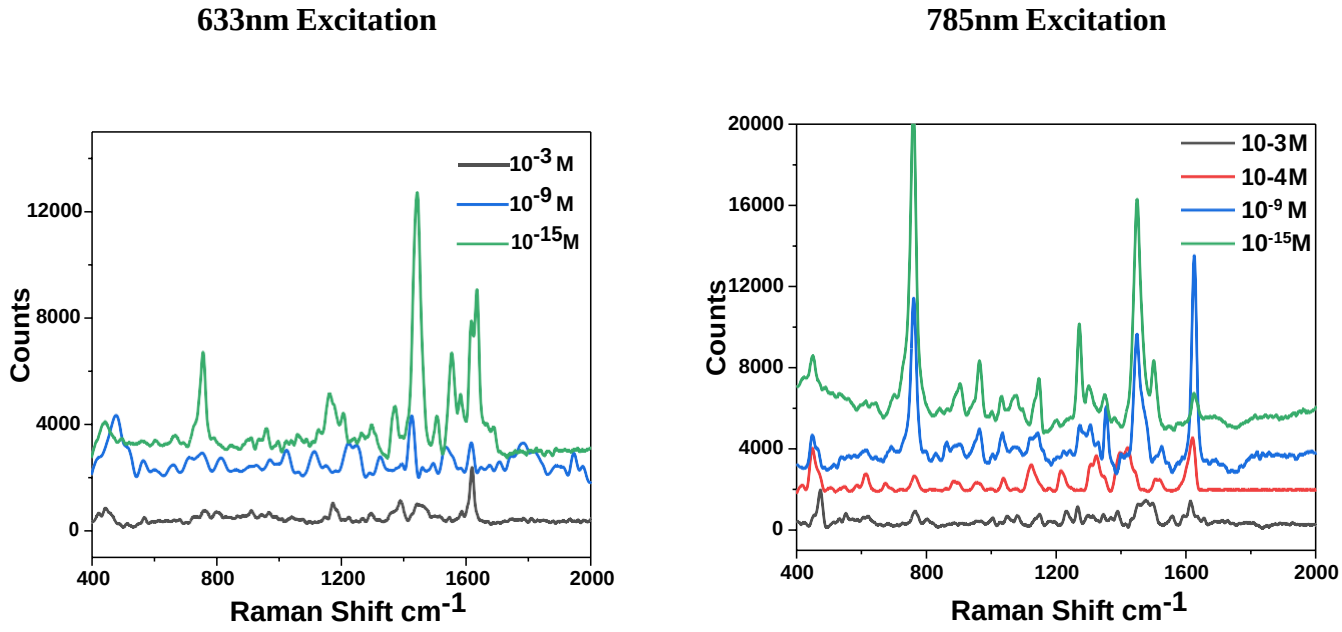

Figure 25. SERS spectra of Spiky shell-hollow Ag@Au core

Figure 26 shows the SERS spectra of Smooth shell- hollow Ag@Au core, and the concentration of MB was varied from 10^{-4}-10^{-8}M.

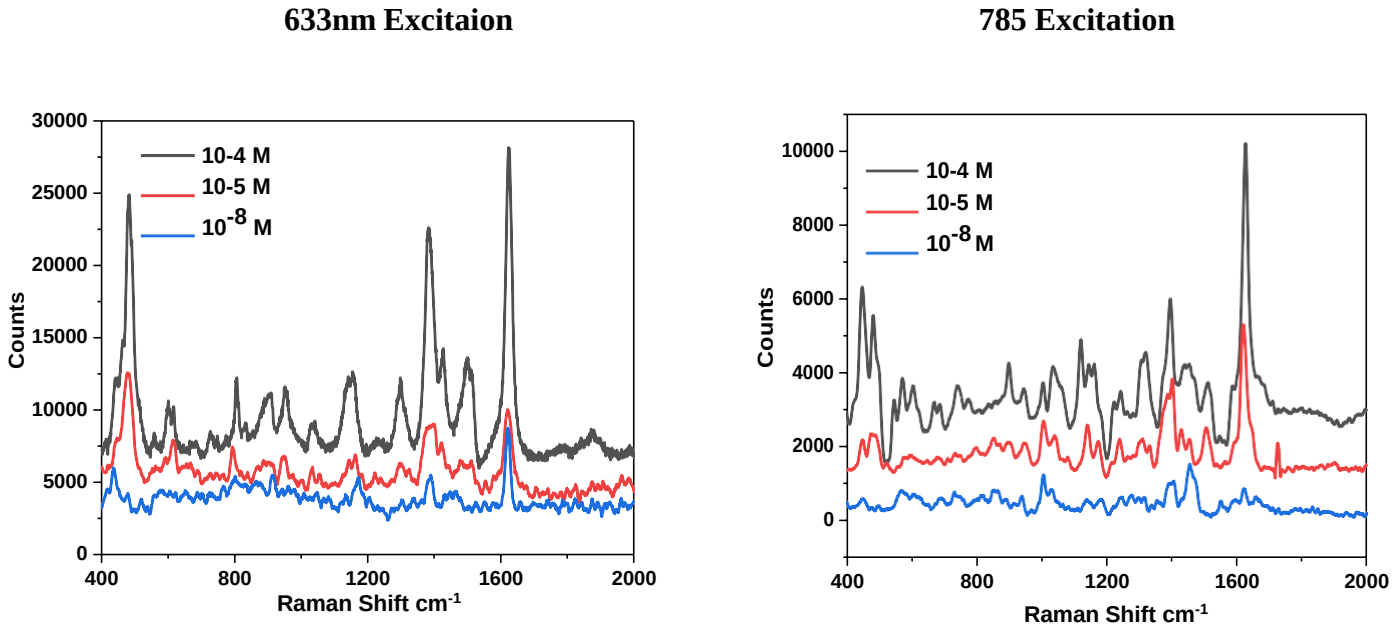

Figure 26. SERS spectra of Smooth shell-hollow Ag@Au core

SERS spectra of Spiky shell-Au solid core was taken at both the excitation wavelength and concentration of MB was varied from 10^{-4}-10^{-8}M. Among the raman shifts, highly enhanced peaks are at 1618, 1444, 1181, 450 cm^{-1} which corresponds to (C-C or C-N stretch), (N-C-H, C-C ring), (C-H_3 stretch), (C-N-C stretch) respectively. The SERS spectra obtained from spiky shell-hollow core was significant due to its special morphology as it has shown peaks even at very low concentration i.e. 10^{-15}M that corresponds to the greater plasmonic enhancement due to the hybridization of plasmon modes of hollow inner region and outer spikes made of gold. In case of smooth shell-hollow core, there is decrease in the intensity of peaks when the concentration of MB was decreased to 10^{-8}M.

SERS spectra of Spiky shell-Au solid core was measured at both the excitation sources and concentration of MB was varied from 10^{-4}-10^{-8}M. (Figure 27)

633nm Excitation **785nm Excitation**

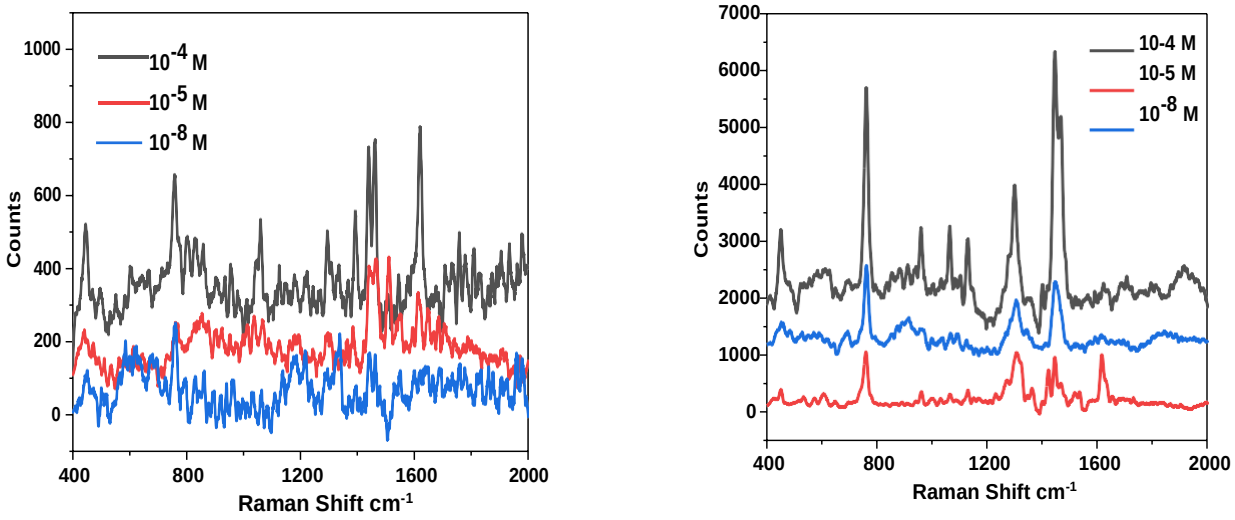

Figure 27. SERS spectra of Spiky shell- Au solid core

The SERS peaks that enhanced were at 1444cm^{-1} (N-C-H, C-C ring), 1392 cm^{-1} (C-N stretch), 769 cm^{-1} (C-H ring). Figure 28 shows the SERS spectra of Smooth shell-Au solid core and concentration of analyte molecule was varied from 10^{-4}-10^{-8}M. The peak intensity decreased on decreasing the concentration as the electric field enhancement in case of solid Au core with smooth shell was less as compared to spiky shell.

633nm Excitation **785nm Excitation**

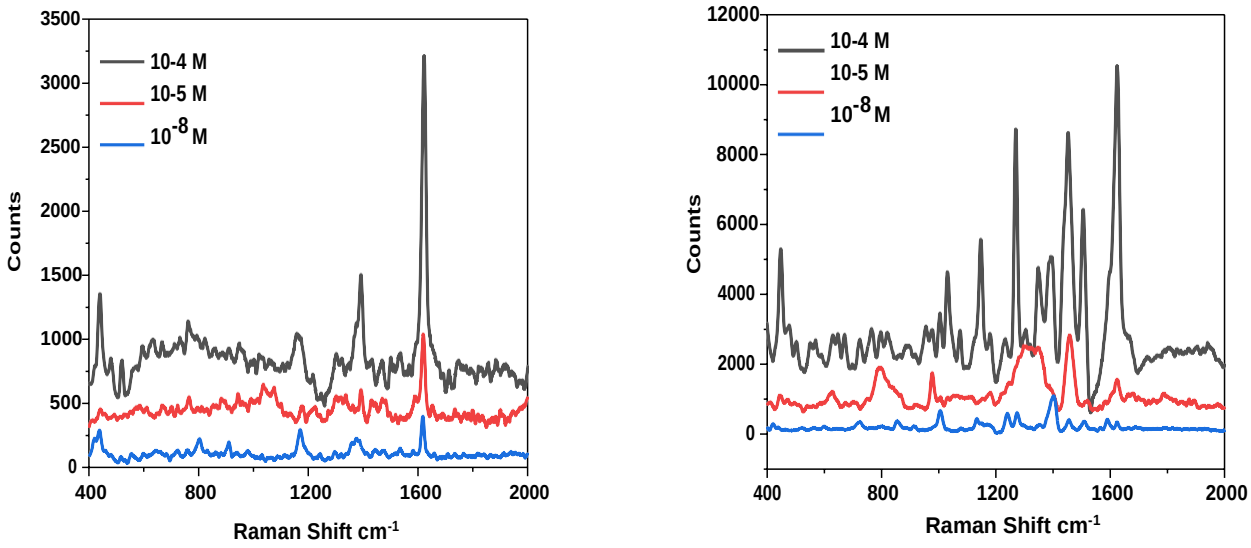

Figure 28. SERS spectra of Smooth shell-Au solid core

We then compared the SERS activity of analyte molecules attached to the outer tips of the spiky core shell nanostructures with the molecules residing in between the core and the spiky shell. Figure 29 shows the SERS spectra when the dye molecules were inside and outside of the spiky core-shell nanostructures and the concentration of dye used was 10^{-5}M using 785nm excitation source. Clearly the intensity of raman peaks when the dye was attached to outer tips of spiky shell was greater than when the molecules were inside reason being tips shows higher electric field enhancement.

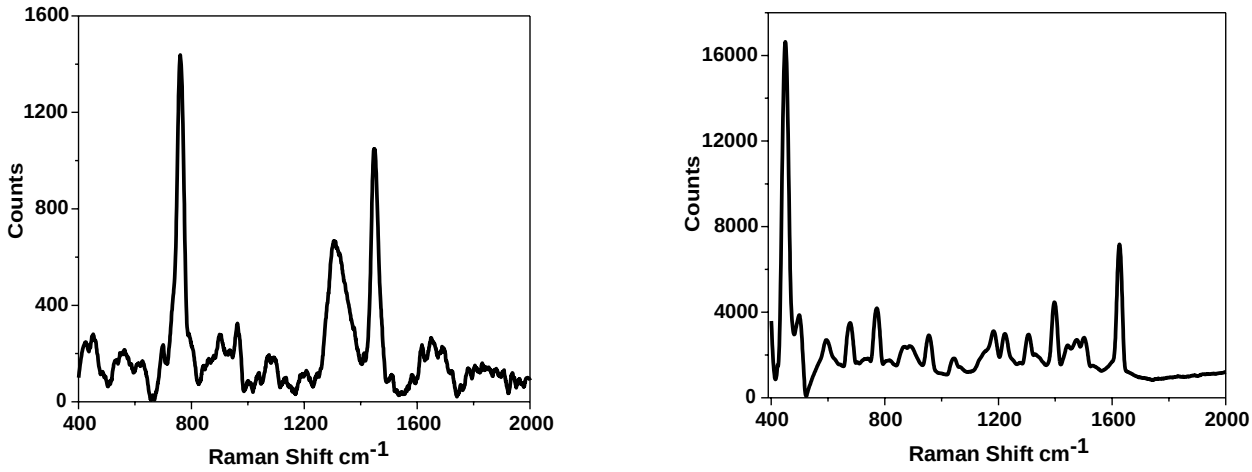

Figure 29. SERS spectra of dye molecules inside and outside of spiky core-shell nanostructures

As these spiky shell-hollow Ag@Au nanostructures can detect upto very low concentrations i.e. pico and femto molar, so to check the reproducibility of these spiky core shell nanostructures SERS signal was measured using very low concentrations under 785nm excitation source. (Figure 30)

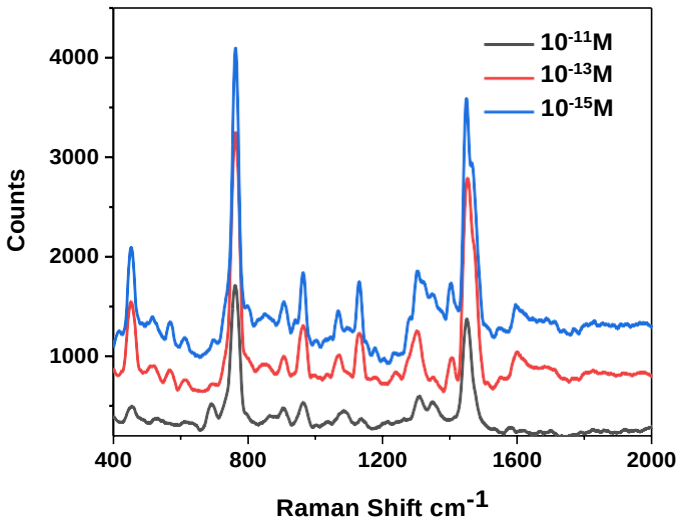

Figure 30. SERS spectra of hollow core-spiky shell at very low concentrations

3.5 Conclusion

We have successfully synthesized core-shell nanostructures comprising of spiky shell and smooth shell-hollow Ag@Au core and spiky and smooth shell-solid Au core. The spiky shell-hollow Ag@Au core showed higher SERS intensity on comparing to their smooth shell and solid core counterpart when the dye molecules were placed between the core and shell and also on the tips of the spiky shell. This greater SERS intensity corresponds to the higher electric field enhancement due to the hybridization of plasmonic modes of core and shell also from the tips of spiky shell. These nanostructures have facilitated the increased raman signal and can be used for single molecule sensing. Thus with enhanced SERS intensity these core-shell nanostructures can be used as an improved platform for therapeutic and bioimaging applications.

Bibliography

(1) Unser, S.; Bruzas, I.; He, J.; Sagle, L. Localized Surface Plasmon Resonance Biosensing: Current Challenges and Approaches. **2015**, 15684–15716. https://doi.org/10.3390/s150715684.

(2) Taylor, P.; Katyal, J.; Soni, R. K. Size- and Shape-Dependent Plasmonic Properties of Aluminum Nanoparticles for Nanosensing Applications. **2013**, No. November 2014, 37–41. https://doi.org/10.1080/09500340.2013.856483.

(3) Hao, E.; Schatz, G. C.; Hupp, J. T. Synthesis and Optical Properties of Anisotropic Metal Nanoparticles. **2004**, *14* (4).

(4) Polavarapu, L.; Pérez-Juste, J.; Xu, Q. H.; Liz-Marzán, L. M. Optical Sensing of Biological, Chemical and Ionic Species through Aggregation of Plasmonic Nanoparticles. *J. Mater. Chem. C* **2014**, *2* (36), 7460–7476. https://doi.org/10.1039/c4tc01142b.

(5) Lertvachirapaiboon, C.; Baba, A. Distance-Dependent Surface Plasmon Resonance Coupling Between a Gold Grating Surface and Silver Nanoparticles. **2014**. https://doi.org/10.1007/s11468-014-9695-2.

(6) Bora, T. Recent Developments on Metal Nanoparticles for SERS Recent Developments on Metal Nanoparticles Applications for SERS Applications. https://doi.org/10.5772/intechopen.71573.

(7) Mcquillan, A. J. The Discovery of Surface-Enhanced Raman Scattering. **2014**, *63* (1), 105–109.

(8) Schatz, G. C. Richard P. Van Duyne (1945–2019). *Nat. Nanotechnol.* **2019**, *14* (August), 41565. https://doi.org/10.1038/s41565-019-0545-4.

(9) Sugawa, K.; Akiyama, T.; Tanoue, Y.; Harumoto, T.; Yanagida, S.; Yasumori, A.; Tomita, S.; Otsuki, J. Particle Size Dependence of the Surface-Enhanced Raman Scattering Properties of Densely Arranged. *Phys. Chem. Chem. Phys.* **2014**. https://doi.org/10.1039/C4CP05058D.

(10) He, R. X.; Liang, R.; Peng, P.; Zhou, Y. N. Effect of the Size of Silver Nanoparticles on SERS Signal Enhancement. **2017**. https://doi.org/10.1007/s11051-017-3953-0.

(11) Reguera, J.; Langer, J.; Jiménez De Aberasturi, D.; Liz-Marzán, L. M. Anisotropic Metal Nanoparticles for Surface Enhanced Raman Scattering. *Chem. Soc. Rev.* **2017**, *46* (13),

3866–3885. https://doi.org/10.1039/c7cs00158d.

(12) Lahr, R. H.; Vikesland, P. J. Surface-Enhanced Raman Spectroscopy (SERS) Cellular Imaging of Intracellularly Biosynthesized Gold Nanoparticles Surface-Enhanced Raman Spectroscopy (SERS) Cellular Imaging of Intracellulary Biosynthesized Gold Nanoparticles. **2014**. https://doi.org/10.1021/sc500105n.

(13) Quester, K.; Avalos-borja, M.; Vilchis-nestor, A. R.; Camacho-lópez, M. A. SERS Properties of Different Sized and Shaped Gold Nanoparticles Biosynthesized under Different Environmental Conditions by Neurospora Crassa Extract. **2013**, *8* (10), 4–11. https://doi.org/10.1371/journal.pone.0077486.

(14) Sun, D.; Zhang, G.; Jiang, X.; Huang, J.; Jing, X.; Zheng, Y.; He, J.; Li, Q. Biogenic Flower-Shaped Au-Pd Nanoparticles: Synthesis, SERS Detection and Catalysis towards Benzyl Alcohol Oxidation. *J. Mater. Chem. A* **2014**, *2* (6), 1767–1773. https://doi.org/10.1039/c3ta13922k.

(15) Krajczewski, J.; Kudelski, A. Shell-Isolated Nanoparticle-Enhanced Raman Spectroscopy. **2019**, *7* (June), 1–6. https://doi.org/10.3389/fchem.2019.00410.

(16) Wilson, O. M.; Knecht, M. R.; Garcia-martinez, J. C.; Crooks, R. M. Effect of Pd Nanoparticle Size on the Catalytic Hydrogenation of Allyl Alcohol. **2006**, 4510–4511.

(17) Li, Y.; Fan, X.; Qi, J.; Ji, J.; Wang, S.; Zhang, G.; Zhang, F. Palladium Nanoparticle-Graphene Hybrids as Active Catalysts for the Suzuki Reaction. *Nano Res.* **2010**, *3* (6), 429–437. https://doi.org/10.1007/s12274-010-0002-z.

(18) Silva, A. G. M.; Rodrigues, T. S.; Wang, J.; Yamada, L. K.; Alves, T. V; Ornellas, F. R.; Ando, R. A.; Camargo, P. H. C. The Fault in Their Shapes: Investigating the Surface-Plasmon- Resonance-Mediated Catalytic Activities of Silver Quasi-Spheres, Cubes, Triangular Prisms, and Wires. **2015**. https://doi.org/10.1021/acs.langmuir.5b02838.

(19) Wang, R.; He, H.; Liu, L.; Dai, H.; Zhao, Z. Catalysis Science & Technology Shape-Dependent Catalytic Activity of Palladium Nanocrystals for the Oxidation of Carbon Monoxide W. **2012**, 575–580. https://doi.org/10.1039/c2cy00417h.

(20) Chowdhury, S. R.; Roy, P. S.; Bhattacharya, S. K. Room Temperature Synthesis of Polyvinyl Alcohol Stabilized Palladium Nanoparticles: Solvent Effect on Shape and Electro-Catalytic Activity. *Nano-Structures and Nano-Objects* **2018**, *14*, 11–18. https://doi.org/10.1016/j.nanoso.2018.01.004.

(21) Wang, F.; Hao, G.; Guo, Y.; Ma, X.; Yang, L. Solvent Effects on Preparation of Pd-Based Catalysts : Influence on Properties of Palladium and Its Catalytic Activity for Benzyl Alcohol Oxidation. **2017**, 59–68. https://doi.org/10.4236/ojmetal.2017.74005.

(22) Chemistry, O. SUZUKI–MIYAURA COUPLING ON HETEROGENEOUS PALLADIUM CATALYSTS Attila Papp, Diána Tóth and Árpád Molnár *. **2006**, *87* (2), 335–342.

(23) Narayanan, R. Recent Advances in Noble Metal Nanocatalysts for Suzuki and Heck Cross-Coupling Reactions. **2010**, 2124–2138. https://doi.org/10.3390/molecules15042124.

(24) Chen, Y.; He, B.; Huang, T.; Liu, H. Controlled Synthesis of Palladium Icosahedra Nanocrystals by Reducing H2PdCl4 with Tetraethylene Glycol. *Colloids Surfaces A Physicochem. Eng. Asp.* **2009**, *348* (1–3), 145–150. https://doi.org/10.1016/j.colsurfa.2009.07.007.

(25) Nadagouda, M. N.; Polshettiwar, V.; Varma, R. S. Self-Assembly of Palladium Nanoparticles: Synthesis of Nanobelts, Nanoplates and Nanotrees Using Vitamin B1, and Their Application in Carbon-Carbon Coupling Reactions. *J. Mater. Chem.* **2009**, *19* (14), 2026–2031. https://doi.org/10.1039/b817112b.

(26) Lee, Y. W.; Woo, S. Shaping Pd Nanocatalysts through the Control of Reaction Sequence W. **2010**, 1535–1537. https://doi.org/10.1039/b920523c.

(27) Soni, K. C.; Krishna, R.; Chandra Shekar, S.; Singh, B. Catalytic Oxidation of Carbon Monoxide over Supported Palladium Nanoparticles. *Appl. Nanosci.* **2016**, *6* (1), 7–17. https://doi.org/10.1007/s13204-015-0419-5.

(28) Di Pietrantonio, K.; Coccia, F.; Tonucci, L.; D'Alessandro, N.; Bressan, M. Hydrogenation of Allyl Alcohols Catalyzed by Aqueous Palladium and Platinum Nanoparticles. *RSC Adv.* **2015**, *5* (84), 68493–68499. https://doi.org/10.1039/c5ra13840j.

(29) Editorial, G. Membrane Reactors – Part I. *Technology* **2009**, No. 17, 111–137. https://doi.org/10.1002/apj.

(30) Kannan, P.; Maiyalagan, T.; Opallo, M. One-Pot Synthesis of Chain-like Palladium Nanocubes and Their Enhanced Electrocatalytic Activity for Fuel-Cell Applications. *Nano Energy* **2013**, *2* (5), 677–687. https://doi.org/10.1016/j.nanoen.2013.08.001.

(31) Cao, M.; Wei, Y.; Gao, S.; Cao, R. Synthesis of Palladium Nanocatalysts with Cucurbit[n]Uril as Both a Protecting Agent and a Support for Suzuki and Heck Reactions.

Catal. Sci. Technol. **2012**, *2* (1), 156–163. https://doi.org/10.1039/c1cy00324k.

(32) Rajendar Reddy, K.; Rajanna, K. C.; Uppalaiah, K. Environmentally Benign Contemporary Friedel-Crafts Acylation of 1-Halo-2-Methoxynaphthalenes and Its Related Compounds under Conventional and Nonconventional Conditions. *Tetrahedron Lett.* **2013**, *54* (26), 3431–3436. https://doi.org/10.1016/j.tetlet.2013.04.075.

(33) Reddy, K. R.; Sana, S.; Uppalaiah, K.; Rajanna, K. C.; Veerasomaiah, P. Environmentally Benign Electrophilic Halogenation of Naphthalenes by H₂O₂—Alkali Metal Halides in An Aqueous Cationic Micellar Media. *Int. J. Org. Chem.* **2012**, *02* (03), 254–261. https://doi.org/10.4236/ijoc.2012.23034.

(34) Xia, Y.; Xiong, Y.; Lim, B.; Skrabalak, S. E. Shape-Controlled Synthesis of Metal Nanocrystals: Simple Chemistry Meets Complex Physics? *Angew. Chemie - Int. Ed.* **2009**, *48* (1), 60–103. https://doi.org/10.1002/anie.200802248.

(35) Gawande, M. B.; Bonifácio, V. D. B.; Luque, R.; Branco, P. S.; Varma, R. S. Benign by Design: Catalyst-Free in-Water, on-Water Green Chemical Methodologies in Organic Synthesis. *Chem. Soc. Rev.* **2013**, *42* (12), 5522–5551. https://doi.org/10.1039/c3cs60025d.

(36) Malassis, L.; Dreyfus, R.; Murphy, R. J.; Hough, L. A.; Donnio, B.; Murray, C. B. One-Step Green Synthesis of Gold and Silver Nanoparticles with Ascorbic Acid and Their Versatile Surface Post-Functionalization. *RSC Adv.* **2016**, *6* (39), 33092–33100. https://doi.org/10.1039/c6ra00194g.

(37) Singh, R. K.; Duvedi, R. Environment-Friendly Green Chemistry Approaches for an Efficient Synthesis of 1-Amidoalkyl-2-Naphthols Catalyzed by Tannic Acid. *Arab. J. Chem.* **2018**, *11* (1), 91–98. https://doi.org/10.1016/j.arabjc.2014.08.022.

(38) Naz, S.; Khaskheli, A. R.; Aljabour, A.; Kara, H.; Talpur, F. N.; Sherazi, S. T. H.; Khaskheli, A. A.; Jawaid, S. Synthesis of Highly Stable Cobalt Nanomaterial Using Gallic Acid and Its Application in Catalysis. *Adv. Chem.* **2014**, *2014*, 1–6. https://doi.org/10.1155/2014/686925.

(39) Nikoobakht, B.; El-Sayed, M. A. Evidence for Bilayer Assembly of Cationic Surfactants on the Surface of Gold Nanorods. *Langmuir* **2001**, *17* (20), 6368–6374. https://doi.org/10.1021/la010530o.

(40) Zhang, A.; Liu, M.; Liu, M.; Xiao, Y.; Li, Z.; Chen, J.; Sun, Y.; Zhao, J.; Fang, S.; Jia, D.;

Li, F. Homogeneous Pd Nanoparticles Produced in Direct Reactions: Green Synthesis, Formation Mechanism and Catalysis Properties. *J. Mater. Chem. A* **2014**, *2* (5), 1369–1374. https://doi.org/10.1039/c3ta14299j.

(41) Ren, J.; Tilley, R. D. Shape-Controlled Growth of Platinum Nanoparticles. *Small* **2007**, *3* (9), 1508–1512. https://doi.org/10.1002/smll.200700135.

(42) Teng, X.; Liang, X.; Maksimuk, S.; Yang, H. Synthesis of Porous Platinum Nanoparticles. *Small* **2006**, *2* (2), 249–253. https://doi.org/10.1002/smll.200500244.

(43) Can, M. Green Synthesis of Pd Nanoparticles via Gallic Acid. *Acta Phys. Pol. A* **2017**, *131* (3), 569–570. https://doi.org/10.12693/APhysPolA.131.569.

(44) Meena Kumari, M.; Aromal, S. A.; Philip, D. Synthesis of Monodispersed Palladium Nanoparticles Using Tannic Acid and Its Optical Non-Linearity. *Spectrochim. Acta - Part A Mol. Biomol. Spectrosc.* **2013**, *103*, 130–133. https://doi.org/10.1016/j.saa.2012.11.020.

(45) Wrigglesworth, E. G.; Johnston, J. H. The Use of Dual Reductants in Gold Nanoparticle Syntheses. *RSC Adv.* **2017**, *7* (72), 45757–45762. https://doi.org/10.1039/c7ra07724f.

(46) Zanda, M.; Vilaró, M.; Barluenga, J. Arylation of Phe and Tyr Side Chains of Unprotected Peptides by a Suzuki-Miyaura Reaction in Water. *Synthesis (Stuttg).* **2009**, No. 3, 14–16. https://doi.org/10.1055/s-0028-1083328.

(47) Littke, A. F.; Dai, C.; Fu, G. C. Versatile Catalysts for the Suzuki Cross-Coupling of Arylboronic Acids with Aryl and Vinyl Halides and Triflates under Mild Conditions. **2000**, No. 9, 4020–4028.

(48) Zorzan, D. FULL PAPER A Mild and Versatile Method for Palladium-Catalyzed Cross-Coupling of Aryl Halides in Water and Surfactants Antonio Arcadi ,* [a] Giorgio Cerichelli ,* [a] Marco Chiarini , [a] Mariano Correa , [a] And. **2003**. https://doi.org/10.1002/ejoc.200300356.

(49) Doria, Y.; Lachguar, A.; Mouton, C.; Daran, J. Inorganica Chimica Acta Phosphine / N-Heterocyclic Carbene Palladium Complex for Suzuki-Miyaura Cross-Coupling Reactions : The Role of Water on Activity. *Inorganica Chim. Acta* **2019**, *492* (April), 91–97. https://doi.org/10.1016/j.ica.2019.04.021.

(50) Liu, X.; Xu, W.; Xiang, D.; Zhang, Z.; Chen, D.; Hu, Y. Palladium Immobilized on Functionalized Hypercrosslinked Polymers : A Highly Active and Recyclable Catalyst for Suzuki – Miyaura Coupling Reactions in Water †. **2019**.

https://doi.org/10.1039/c9nj02444a.

(51) Wallow, T. I. Highly Efficient and Accelerated Suzuki Aryl Couplings Mediated by Phosphine-Free Palladium Sources. **2013**, No. 11, 5034–5037.

(52) Bej, A.; Ghosh, K.; Sarkar, A.; Knight, D. W. RSC Advances Palladium Nanoparticles in the Catalysis of Coupling Reactions. **2016**, No. c, 11446–11453. https://doi.org/10.1039/c5ra26304b.

(53) Han, W.; Liu, C.; Jin, Z. In Situ Generation of Palladium Nanoparticles : A Simple and Highly Active Protocol for Oxygen-Promoted Ligand-Free Suzuki Coupling Reaction of Aryl Chlorides. **2007**, No. d, 2006–2008.

(54) Chemistry, O. Efficient , Selective , and Recyclable Palladium Catalysts in Carbon - Carbon Coupling Reactions Rp. **2011**, 2251–2320.

(55) Jin, M.; Taher, A.; Kang, H.; Ryoo, R. Palladium Acetate Immobilized in a Hierarchical MFI Zeolite-Supported Ionic Liquid : A Highly Active and Recyclable Catalyst for Suzuki Reaction in Water. **2009**, *1*, 309–313. https://doi.org/10.1039/b817855k.

(56) Karimi, B.; Mansouri, F.; Vali, H. Anchored TEG-Imidazolium Ionic Liquid for the Suzuki – Miyaura Coupling Reaction in Water †. **2014**, 2587–2596. https://doi.org/10.1039/c3gc42311e.

(57) Yang, Y.; Castano, C. E.; Gupton, B. F.; Reber, A. C.; Khanna, S. N. As Featured In : **2016**. https://doi.org/10.1039/c6nr06793j.

(58) Collins, G.; Schmidt, M.; Mcglacken, G.; Holmes, J. D. Enhanced Catalytic Activity of High-Index Faceted Palladium Nanoparticles in Suzuki − Miyaura Coupling Due to E Ffi Cient Leaching Mechanism. **2014**. https://doi.org/10.1021/cs5008014.

(59) Zotto, A. Del; Zuccaccia, D. Catalysis Science & Technology Coupling Reaction : A Unified View of the Process of Solution. **2017**, 3934–3951. https://doi.org/10.1039/c7cy01201b.

(60) Ren, L. Z.; Meng, L. J. Suzuki Coupling Reactions Catalyzed by Poly (N-Ethyl-4-Vinylpyridinium) Bromide Stabilized Palladium Nanoparticles in Aqueous Solution. **2008**, *2* (4), 251–255. https://doi.org/10.3144/expresspolymlett.2008.30.

(61) Chen, Y.; Hung, H.; Huang, M. H. Seed-Mediated Synthesis of Palladium Nanorods and Branched Nanocrystals and Their Use as Recyclable Suzuki Coupling Reaction Catalysts. **2009**, No. 11, 9114–9121.

(62) Fujii, S.; Matsuzawa, S.; Nakamura, Y.; Ohtaka, A.; Teratani, T. Synthesis and Characterization of Polypyrrole - Palladium Nanocomposite-Coated Latex Particles and Their Use as a Catalyst for Suzuki Coupling Reaction in Aqueous Media. **2010**, *26* (13), 6230–6239. https://doi.org/10.1021/la9039545.

(63) Kim, S.; Kim, M.; Lee, W. Y.; Hyeon, T. Fabrication of Hollow Palladium Spheres and Their Successful Application to the Recyclable Heterogeneous Catalyst for Suzuki Coupling Reactions. **2002**, 7642–7643. https://doi.org/10.1021/ja026032z.

(64) Elazab, H. A. Microwave-Assisted Synthesis of Palladium Nanoparticles Supported on Copper Oxide in Aqueous Medium as an Efficient Catalyst for Suzuki Cross-Coupling Reaction. **2018**. https://doi.org/10.1177/0263617418771777.

(65) Shen, H.; Shen, C.; Chen, C.; Zhang, P. Catalysis Science & Technology Nanoparticles : Efficient and Recoverable Catalysts. **2015**, 2065–2071. https://doi.org/10.1039/c5cy00013k.

(66) Kuniyil, M.; Kumar, J. V. S.; Adil, S. F.; Shaik, M. R.; Khan, M.; Assal, M. E.; Siddiqui, M. R. H.; Al-warthan, A. One-Pot Synthesized Pd @ N-Doped Graphene : An. **2019**, 1–14.

(67) Miyaura, S.; Reaction, C.; Ahadi, A.; Rostamnia, S.; Panahi, P.; Wilson, L. D.; Kong, Q. Supported Periodic Mesoporous Organosilica (PMO): Pd @ Bipy – PMO as an Efficient Hybrid Catalyst For. https://doi.org/10.3390/catal9020140.

(68) Sci, C.; Islam, R. U.; Witcomb, M. J.; Scurrell, M. S. Catalysis Science & Technology Conjugated Polymer Stabilized Palladium Nanoparticles as a Versatile Catalyst for Suzuki Cross-Coupling Reactions for Both Aryl and Heteroaryl Bromide Systems. **2011**, 308–315. https://doi.org/10.1039/c0cy00071j.

(69) Cao, M.; Wei, Y.; Gao, S.; Cao, R. Catalysis Science & Technology Synthesis of Palladium Nanocatalysts with Cucurbit [n] Uril as Both a Protecting Agent and a Support for Suzuki and Heck Reactions W. **2012**, 156–163. https://doi.org/10.1039/c1cy00324k.

(70) El-sayed, N.; Trouillet, V.; Clasen, A.; Jung, G.; Hollemeyer, K.; Schneider, M. NIR-Emitting Gold Nanoclusters – Modified Gelatin Nanoparticles as a Bioimaging Agent in Tissue. **2019**, *1900993*. https://doi.org/10.1002/adhm.201900993.

(71) Nanoplasmonic Alloy of Au / Ag Nanocomposites on Paper Substrate for Biosensing Applications. **2017**. https://doi.org/10.1021/acsami.7b16182.

(72) Starowicz, Z.; Ozga, P.; Sheregii, E. M. The Tuning of the Plasmon Resonance of the Metal

Nanoparticles in Terms of the SERS Effect. **2018**.

(73) Mclellan, J. M.; Siekkinen, A.; Chen, J.; Xia, Y. Comparison of the Surface-Enhanced Raman Scattering on Sharp and Truncated Silver Nanocubes. **2006**, *427*, 122–126. https://doi.org/10.1016/j.cplett.2006.05.111.

(74) Qi, Y.; Xing, T.; Zhao, J.; Weng, G.; Li, J.; Zhu, J.; Zhao, J. Tuning the Surface Enhanced Raman Scattering Performance of Anisotropic Au Core À Ag Shell Hetero-Nanostructure : The Effect of Core Geometry. *J. Alloys Compd.* **2019**, *776*, e1331–e1336. https://doi.org/10.1016/j.jallcom.2018.10.321.

(75) Fern, M.; Rodr, G.; Camacho-l, C. M. Ac Ce p Cr T. *Appl. Surf. Sci.* **2015**. https://doi.org/10.1016/j.apsusc.2015.01.075.

(76) Luo, Z.; Chen, K.; Lu, D.; Han, H. Synthesis of P-Aminothiophenol-Embedded Gold / Silver Core-Shell Nanostructures as Novel SERS Tags for Biosensing Applications. **2011**, *2*, 149–156. https://doi.org/10.1007/s00604-010-0537-4.

(77) Lim, D.; Jeon, K.; Hwang, J.; Kim, H.; Kwon, S.; Suh, Y. D.; Nam, J. Nanoparticles with 1-Nm Interior Gap. *Nat. Nanotechnol.* **2011**, No. May, 1–9. https://doi.org/10.1038/nnano.2011.79.

(78) Jana, D.; Gorunmez, Z.; He, J.; Bruzas, I.; Beck, T.; Sagle, L. Debrina Jana, † , § Zohre Gorunmez, ‡ , § Jie He, † Ian Bruzas, † Thomas Beck, ‡ , † and Laura Sagle * , † †. **2016**. https://doi.org/10.1021/acs.jpcc.6b02135.

(79) Nerambourg, N.; Werts, M. H. V; Blanchard-desce, M. Distance-Dependent Fluorescence Quenching on Gold Nanoparticles Ensheathed with Layer-by-Layer Assembled Polyelectrolytes. **2006**.

(80) Chee, S. W.; Tan, S. F.; Baraissov, Z.; Bosman, M.; Mirsaidov, U. Direct Observation of the Nanoscale Kirkendall Effect during Galvanic Replacement Reactions. *Nat. Commun.* 1–8. https://doi.org/10.1038/s41467-017-01175-2.